Upstream migrating knickpoints and related sedimentary processes in a submarine canyon from a rare 20-year morphobathymetric time-lapse (Capbreton submarine canyon, Bay of Biscay, France)

Léa GUIASTRENNEC-FAUGAS(1), Hervé GILLET(1), Ricardo SILVA JACINTO(2), Bernard DENNIELOU(2), Vincent HANQUIEZ(1), Sabine SCHMIDT(1), Laure SIMPLET(2), Antoine ROUSSET(1)

(1) Université de Bordeaux, UMR 5805 EPOC, Allée Geoffroy Saint-Hilaire, 33615 Pessac Cedex, France

(2) IFREMER/Brest, BP70, 29280 Plouzané, France

ABSTRACT

The Capbreton submarine canyon is a striking feature of the south-east of the Bay of Biscay. This canyon forms a deep incision through the continental shelf and slope, and displays remarkable structures linked to its present-day hydrosedimentary activity. Its head has been disconnected from the Adour River since 1310 AD, but remains close enough to the coast to be supplied with sediment by longshore drift. Gravity processes in the canyon body are abundantly described and documented, but activity in the head and the fan of the canyon is poorly constrained. Furthermore, many questions remain regarding the details of processes affecting the head, the body and the fan of the Capbreton canyon. In this work, we address the paucity of documentation concerning (1) the temporal evolution of sediment transfer between the head and the deep reaches of the canyon, and (2) the interaction between gravity processes and the morphology of the canyon floor, including both shaping and feedback mechanisms.

This study is based on the analysis and comparison of eight multibeam bathymetric surveys acquired in the upper part of the Capbreton canyon between 1998 and 2018, in depths ranging 10-320 m below sea level. This rare time series exposes the morphological evolution of this outstanding dynamic area over the last 20 years. Our work shows that much of the changes are located in the canyon floor and head. Following a period characterised by a unique flat floor thalweg, the canyon was affected by an incision with low lateral terraces which resulted in a narrow axial thalweg. The deepening of the narrow thalweg was induced by retrogressive erosion according to the presence of upstream-migrating knickpoints, while low elevation residual terraces formed as the canyon reached a local equilibrium profile.

The flat thalweg observed in 1998 is likely a result of a partial filling of the canyon thalweg by a substantial emptying of the canyon head and significant mass transfer to the proximal part of the canyon. A flat floor thalweg was not observed again in the remaining of our time series (since 2010), suggesting a possible quieter working mode of the canyon. We also propose the first accurate volume quantification of sediment displacement on the canyon floor. Our findings underline the alternation of filling and erosive periods in the canyon axis and an unexpected continuous sediment deposition in the canyon head during the last 20 years.

Keywords: Submarine canyon; bathymetric time-lapse; morphobathymetry; knickpoints

1. INTRODUCTION

Submarine canyons are ubiquitous on continental margins (e.g. Shepard, 1981). Studies in various environments (both silicoclastic and carbonate) have demonstrated that they are preferential pathways of terrigenous sediment from rivers and littoral zones to the deep sea during both lowstands and highstands (Shepard and Dill, 1966; Shepard, 1981; Durrieu de Madron, 1994; Mullenbach and Nittrouer, 2000; Puig et al., 2008; Maier et al., 2018). Submarine canyons are complex morphologic elements dominated by erosional processes. Their formation includes erosion by particle-laden gravity currents (Shepard, 1981; Pratson et al., 1994) and subsequent destabilization of flanks (Sultan et al., 2007; Mulder et al., 2017) and is modulated by generated depositional environments such as meander bars and terraces (Babonneau et al., 2002, 2004, 2010; Conway et al., 2012). However, studies are commonly based on static morphologies that do not allow to distinguish inherited morphologies (for instance, during the last glacial lowstand) from present (interglacial high-stand) hydro-sedimentary processes. Pioneering works, based on fixed morphology through seismic profiles (Hay, 1987) and sediment cores (Nesteroff and Heezen, 1962), allow the good understanding of different canyon types and their functioning. Over the last 20 years, current meter and sediment trap moorings (Xu et al., 2002; Khripounoff et al., 2003; Paull et al., 2002; Lintern et al., 2016; Zhang et al., 2018), repeated bathymetric surveys (Smith et al., 2005, 2007; Xu et al., 2008; ; Hughes Clarke et al., 2014; Lintern et al., 2016; Hage et al., 2018; Yin et al., 2019) and direct observation by ROV (Gillet et al., 2019; Paull et al., 2005; Paull et al., 2010) have contributed to filling the gap between observed morpho-sedimentary features and hydro-sedimentary processes. The monitoring of currents and of seabed morphology of both active canyons that are significantly supplied by sediment during the present high-stand (e.g. Var (Migeon et al., 2006; Khripounoff et al., 2012; Kelner et al., 2016), Congo (Babonneau et al., 2010; Azpiroz-Zabala et al., 2018), Monterey (Smith et al., 2005, 2007)) and sediment starved canyons (Normandeau et al., 2014) has played an integral part in our better understanding of sediment transfer dynamics in canyon settings.

The Capbreton canyon, is an excellent illustration of a system driven by powerful hydrosedimentary processes, in particular storm-induced head-to-middle canyon transport (Mulder et al., 2001), and high sediment supply and accumulation rates throughout the Holocene and during the present time (Salles et al., 2008; Mulder et al., 2012; Brocheray et al., 2014). Our work builds-on a previous study by Mazières et al. (2014) which focused on the head of the Capbreton canyon (5-130 m water depth, between 2001 and 2013) in an effort to document both the dynamics and the hazards related to the close coastal setting of this canyon. The aim of this study is to decipher the sediment transfer from the canyon head to the upper course and characterise the morphological response of these different parts to gravity processes. To address these issues, we analyse the evolution of morphological features (such as bedforms and terraces) and compute the volumes of sediment displaced in the process. Our results concerning the morphological evolution of the canyon led us to discuss the sequence of events involved in reaching a local and transient equilibrium profile. Our approach is based on an annual to pluri-annual investigation over the last 20 years (1998 to 2018), relying on 8 multibeam bathymetric surveys which were used to follow the morpho-sedimentary evolution of the upper Capbreton canyon and its head (10-320 m water depth). This rare time-series has enabled us to focus on (1) the migration velocity of morphologic features such as the backstepping of knickpoints, (2) on the energy and frequency of turbiditic flows and (3) on the construction of sedimentary terraces.

2. REGIONAL SETTING

2.1. MORPHOLOGICAL AND GEOLOGICAL SETTING

The Capbreton canyon is located to the southeast of the Bay of Biscay (SW France, *Figure 1*). It was formed 50-40 My ago, during the Middle Eocene (Ferrer et al., 2008), in a subsiding zone with structural weaknesses generated by the convergence of the Iberian and European plates (Deregnaucourt and Boillot, 1982). Several studies have demonstrated the predominant impact of deep-rooted tectonic structures on the localization and overall morphology of the Capbreton Canyon (Deregnaucourt and Boillot, 1982; Bois et al., 1997; Cirac et al., 2001). Until the Middle Miocene, depositional processes prevailed on the valley floor (sedimentation of overbank, levee and mass flow deposits), leading to a progressive infill and smoothing of the canyon morphology. Since then, canyon erosion and deepening have dominated (Ferrer et al., 2008).

The canyon head is located only 300 m off the coastline and forms a deep and wide amphitheater facing the sea (Froidefond, 1982; Gaudin et al., 2006) (*Figure 1*). The canyon deeply incises the Aquitaine continental shelf and slope and shows a 300-kilometer-long meandering course that runs eastwards, parallel to the north coast of Spain, before heading northwards to the base of the continental slope at 3500 m water depth where it merge with the Cap-Ferret-Capbreton deep-sea fan system (Cremer, 1983; Cirac et al., 2001; Gaudin et al., 2006). It can be categorized as a Type 1 canyon (river-associated, shelf-incising canyon), according to the classification proposed by Harris and Whiteway (2011).

2.2. SEDIMENT SUPPLY

Successive connections and disconnections, especially during the Quaternary, with the Adour and paleo Adour River have been reported by Klingebiel and Legigan (1978). The canyon head was naturally disconnected from the Adour River in 1310 AD, and in 1578 the river mouth was artificially relocated 15 km to the south of the canyon head, interrupting direct sediment transfer from the river (Klingebiel and Legigan, 1978). Despite this disconnection, the Adour River continues to indirectly deliver sediment into the canyon (Brocheray et al., 2014; Mazières et al., 2014). Remote sensing satellite images reveal that over the course of a year, the Adour plume reaches the canyon head 20% of the time. The flux from the Adour River represents 0.25×10^6 t.year^{-1} of suspended sediment which is deflected to the north under the influence of easterly winds (Petus, 2009).

However, the present main sediment source is the southward longshore drift that transports large volumes of sediment toward the canyon head during periods of intense coastal erosion under high-energy wave conditions (Mazières et al., 2014). The head of the Capbreton Canyon acts as a sediment buffer, which temporarily traps fine sands (and some mud) before discharging towards the body of the canyon (Mazières et al., 2014). The annual average of sediment transported along the Aquitaine coast ranges between 38,000 m^3 and 657,000 m^3 (Idier et al., 2013). This figure declines dramatically from approximately 40,000 m^3.year^{-1} just north of the canyon to only 1000 m^3.year^{-1} to the south (Abadie et al., 2006). These natural processes are disturbed by an artificial by-pass system. Since 2008, up to 100 000 m^3 of sand per year from 2008 to 2016, and up to 200 000 m^3 per year since 2016 is pumped from the Notre-Dame Beach (north of the canyon head) onto beaches (Estacade, Centrale, Prévent and Savane) south of the canyon head to reduce costal erosion which is accentuated by the Capbreton port breakwater (CASAGEC Ingénierie, 2016).

Poleward jet currents of up to 55 cm.s^{-1} have been measured along the Aquitaine shelf, at a depth of about 50 m (innershelf), after a few days of westerlies in the south-eastern area of the Bay of Biscay (downwelling circulation induced along the Spanish coast). For the strongest events, current velocities recorded at 54 m water depth increased from 8 to 55 cm/s north of the Capbreton canyon

(44°N) (Kersalé et al., 2016), and from 12 cm/s at the bottom to 32 cm/s near the surface offshore the Arcachon Bay (Batifoulier et al., 2012). These currents are known to transport harmful Dinophysis spp. blooms from the south of the Aquitaine shelf to the Arcachon Bay (Batifoulier et al., 2012), and therefore may also carry fine sediment from the inner shelf to the vicinity of the Capbreton Canyon. In addition, poleward jets may be involved in the transport of fine sediment from the inner shelf to the canyon after resuspension by the tide or internal waves.

2.3. PRESENT HYDRO-SEDIMENTARY ACTIVITIES

The Capbreton Canyon is currently active. Sediment transport is triggered by two types of currents according to Mulder et al. (2012): (1) internal tides generating a particle-laden upstream or deep downstream motion of wave masses along the canyon axis, and (2) low to high energy turbidity currents (mean velocity = 0.2–0.3 and 1–3 $m.s^{-1}$, resp.), which transfer fine to coarse particles towards the deep sea. Turbidites generated during violent storm Martin which occurred on December 27th 1999 demonstrated that sediment transfer in the Capbreton canyon is still efficient despite the recent disconnection of the Adour River from the canyon head (Mulder et al., 2001). Interestingly, an aggradational terrace at 431 m water depth indicates that migrations of the Adour River over the last 2 ka did not have a strong effect on the response of the sedimentological signal (Mary et al., 2015). Sedimentary records evidence that coarse deposits are restricted to the thalweg. The absence of particles coarser than silt above 225 m from the thalweg, indicates that sand spill-over did not exceed this height (Gaudin et al., 2006; Brocheray et al., 2014; Mary et al., 2015). At 1600 m water depth and about 150 km from the canyon head, the frequency of turbiditic deposits is 1,7 and 1,2 turbidites/year at respective altitudes above the thalweg of 75 and 125 m (Brocheray et al., 2014). Upstream, at 647 m water depth and 37 km from the canyon head, reduced frequencies of about 1 turbidite every 10 years (Mulder et al., 2001) were interpreted as poor preservation of deposits due to higher erosion rates (Brocheray et al., 2014).

However, gravity flows in the form of turbidity currents or grain flow, do not appear to be energetic enough to transport the coarse fraction down to the Cap Ferret deep-sea fan (Cremer, 1983). This fraction settles in the upper part of the canyon, which implies that the canyon is currently being filled. The Capbreton canyon morphology has evolved continuously from highstand to lowstand periods, with reduced erosive energy reported during highstands (Gaudin et al., 2006). Under high sea-level conditions, the hydro-sedimentary activity inside a submarine canyon can be triggered by exceptional events such as storms or earthquakes which are prone to initiate gravity flows, while punctual sediment failure can occur outside of these exceptional events (Khripounoff et al., 2012).

3. MATERIALS AND METHODS

This work is based on the analysis and comparison of 8 multibeam bathymetric surveys acquired in spring or summer from 1998 to 2018 (*Figure 2*, *Table 1*). These surveys repeatedly covered the upper area of the canyon from 10 to 320 m water depth. Real Time Kinematic (RTK) GPS was used for the positioning with a horizontal resolution of 0.01 m and a vertical resolution of 0.02 m. Spatial resolution ranges from 0.5 to 5 m, depending on the multibeam echo sounder. The technical staff of RV operators (SHOM or Ifremer/Genavir) used temperature or both temperature and salinity data (from XBT or CDT probes) combined with statistical databases (i.e. WOA09, WOA13 or ISAS; Antonov et al., 2010; Locarnini et al., 2010; Boyer et al., 2013; Kolodziejczyk et al., 2017) to compute sound velocity profile in water column and make real-time correction of the bathymetry. Vertical precision is comprised between 0.2% to 0.4% (depending on the multibeam echo sounder; Table 1) of the water depth with possible biases from 0.02 m to 1.28 m. The bathymetric data were collected and postprocessed using the Ifremer's CARAIBES™ software, including manual editing and automated filters, which allowed for the creation of a final digital elevation model (DEM). Due to the lack of buoys in the part of the Bay of Biscay studied here, tide corrections were made using a tide prediction algorithm from the SHOM (Service Hydrographique et Océanographique de la Marine). All the DEM were reproduced on a common grid with a horizontal resolution of 5 meters in order to enable comparative calculations. Bathymetric differential and volume quantification were performed with a routine developed on ArcGIS for Desktop software (Esri). Using a nearby seabed surface that geologically is extremely unlikely to have changed (exposed consolidated sediment including

authigenic carbonate; Gillet et al., 2019), statistics of repeat survey observations (specifically 206 224 data point couples spaced no more than 1 m apart of non-gridded raw data) over an area about 0.07 km² in depths of 35 to 60 m (Roches Duprat, located on Figure 3C), indicate an inter survey (2012-2018) bias of just 4 cm with variability of +/-17cm. This realization validates the estimated 0.2-0.4% depth uncertainty used to constrain confidence in the inter survey volume estimates used herein.
To better visualize morphological features, the regional bathymetric trends along the canyon floor were subtracted from DEMs. For this purpose, an along canyon floor polynomial surface excluding surrounding shelf and canyon lateral slopes was computed. Resulting compensated DEMs were kept at the best to calculate relative slope and to emphasize morphological fluctuations (Figure 3 A,B).
A 2.1 m-long piston core, KS05, was retrieved during the PROTEVS-DUNES cruise in 2013 (Mathias, 2013) on a terrace with considerable seabed changes during the last 10 years observed in the study area (see localization on *Figure 1*). The study of the core included grain size, X-ray and radionuclide analyses. In order to provide a chronological framework, ^{210}Pb, ^{226}Ra and ^{232}Th activities were measured on selected 1-cm layers of sediment (avoiding sandy horizons) by non-destructive gamma spectrometry using a low-background, high-efficiency, well-type detector (Schmidt et al, 2014). Excess ^{210}Pb was calculated by subtracting the activity supported by its parent isotope (^{226}Ra) from the total ^{210}Pb activity in the sediment. The long-lived ^{232}Th is usually associated with the detrital fraction. Therefore, ^{232}Th activity changes can be an indication of different lithological sources or proportions, and is used here to highlight potential $^{210}Pb_{xs}$ dilution by sand.

4. RESULTS

4.1. OVERALL MORPHOLOGY

The slope of the inner shelf surrounding the canyon head does not exceed 0.5°. On each side of the canyon, and in a seaward direction, lies the following series of rocky shelf outcrops (*Figure 3*C): *roches du champs de la Talère* (south side, 30 m water depth), *roches du Moulin* (north side, 40 water depth), *roches Duprat* (north side, 40 water depth), *roches du Champ des Vaches* (north side, 60 to 70 m water depth) and *roches du Doigt Mordu* (south side, 70 m water depth). The only rock sample recovered in the area by a gravity rock corer on the *roches Duprat* outcrop, was constituted of carbonate-cemented sandstone. According to microfossils analysis (foraminifera and dinocysts), this sample is dated to the Miocene (Londeix, person. comm.).

In this study, both the upper part and the head of the canyon were considered separately. The narrowing between the amphitheater morphology and the channel morphology marks the limit between these two units (Figure 1B). Based on the new 2018 DEM, the head is 1 km long with an amphitheater shape narrowing seaward from a maximum of 1200 m wide at 300 m from the coast at 10 m water depth, to 300 m wide at 1400 m from the coast at 120 m water depth. The average slope of the canyon head is 4.48° and can reach 10° along the first hundred meters. The flanks of the head of the canyon are asymmetric: the southern flank have a slope ranging between 5 and 10° with the shelf break reaching 50°, whereas the northern flank is steeper with slopes of about 12 to 25° but a softer shelf break of about 30°. This overall morphology is similar to that observed on the new DEMs acquired in 2015 and 2016, and to those described in previous studies (Froidefond et al., 1983; Gaudin et al., 2006; Mazières et al., 2014). The sea floor morphology is characterized by the occurrence of groups of bedforms that are morphologically similar in size and shape. These structures were described as Crescent-Shaped Bedforms (CSBs) by Smith et al. (2005) and Paull et al. (2011). The CSBs' wavelengths increase with depth and range from 30 to 50 m with an amplitude of 2 to 8 m.

The upper canyon has a U-shaped cross-section (*Figure 4*A, B) and a width ranging from 75 to 400 m. Several types of morphology of the canyon flanks are distinguished (1) gentle slope (10 to 20°) with smoothed gullies, (2) steep roughly gullied flanks in outer meander flanks (20 to 40°), (3) steep flanks (20 to 40°) with gullies of up to 100 m-wide extending into and incising the surrounding shelf, and (4) meanders with large bend radius and collapsed outer flanks (up to 40°) (*Figure 3*C).

A sinuous channel incises the upper canyon overhung by terraces. Two categories of terraces are distinguished: (1) elongated low elevation terraces which occur 10 to 15 m above the canyon floor in narrow channel bends, and (2) round high elevation terraces found 45 to 100m above the canyon floor in open channel bends (*Figure 3*C).

Based on the bathymetric survey acquired in May 2018 (*Figure 3*A), the canyon floor is characterized by an average slope of 1° along its first eight kilometres. It shows several isolated scarps (steps), hanging at a height of up to 7 m, hereafter referred to as knickpoints.

4.2. TIME-LAPSE MULTIBEAM DATASET ANALYSIS

4.2.1. UPPER CANYON FLOOR EVOLUTION BETWEEN 1998 AND 2018

Between August 1998 and May 2018, the differential bathymetry (*Figure 4*C) highlights the development of a 25 m-deep incision in the canyon floor, and the accumulation of up to 15 m of sediment forming low elevation elongated terraces (LT). A flattened floor is observed in 1998 (*Figure 4*A) and is succeeded by the presence of an incised axial channel bordered by numerous low lateral terraces from 2010 to 2018 (*Figure 3*C; *Figure 4*B; *link to the animation 1*). The last survey of our time series (May 2018) revealed the presence of nine such low elongated lateral terraces (referred to as LT 1 (coastward) to LT 9 (deepward)) in the uppermost part of the canyon , (*Figure 3*C). These terraces were absent in the 1998 morphology (*Figure 4*A) where the canyon floor was much flatter. The formation of these striking features thus began during the 12 year-long hiatus in our dataset between 1998 and 2010, and continued at least until our last survey in May 2018. In addition, new knickpoints appeared in the canyon. From 2010 to 2018, we observed the formation of several features, which evolved and migrated over time. They are dominated by two types of erosion: (1) erosion along the channel floor probably linked to the back stepping of knickpoints, and (2) lateral erosion affecting the low terraces.

Minor evolutions are observed outside the canyon floor (Figure 2; link to the animation 1). Four active dendritic gully networks incising the shelf are observed between 1998 and 2018. Two active gullies, to the east of the *Roches du Doigt Mordu* rocky outcrop, incise the canyon's southern flank. The eastern gully experienced a 205 m retreat on the shelf between 1998 and 2013, while the western one experienced a 485 m retreat between 1998 and 2015. The biggest gully network, previously described by Mazières et al (2014), located in the vicinity of the *Roches du Champ de la Talère*, incises the southern flanks of the canyon head. It experienced a 1015 m retreat between 2001 (no data available for 1998) and 2015, but was quiescent between 2012 and 2013. A second network of steep gullies that incise the northern flank of the canyon (head through the *Roches du Moulin* rock field), was already present in 1998, but experienced a 245 m backstepping between 2013 and 2018. In addition, this gully network cut across the low elevation terrace LT1, and its activity is highlighted by the migration of bedforms down the network between 2015 and 2018 (*link to the animation 1*). Only the *Roches du Moulin* gullies network experienced retreat erosion between 2016 and 2018 (*Figure 3*C).

The morphological evolutions in the upper canyon over the last 20 years especially affected the floor of the canyon and the canyon head. The canyon flanks appear rather stable during the investigated period, for this reason, all results described hereafter focus on the canyon floor.

4.2.3. KNICKPOINTS

Up to 80 knickpoints cover the upper canyon floor (*Figure 3*C). Here, we only describe knickpoints with a minimal height of 1 m and a minimal slope of 5°, in accordance with our bathymetric resolution and to allow the monitoring of knickpoints on the different DEMs through the years. Knickpoints are present all along the studied area with higher occurrence upstream channel bends. Knickpoints height range up to 7 m and slope up to 25°. They are either isolated or coalescent (up to 6 amalgamated knickpoints). Some are characterized by the presence of downstream plunge pools. In the canyon head, knickpoints are also present among CSBs. As described by Paull et al. (2011), knickpoints differ from CSBs by being higher or distinctly narrower than the CSB scarps immediately upstream. The knickpoint scarp marks the beginning of the next group of CSBs further down canyon. The surveys are close enough in time to allow us to monitor the temporal evolution and migration of several significant knickpoints, especially during the 2010-2018 period. The overall evolution of the channel floor morphology is characterized by the upstream migration of knickpoints. The migration velocity ranges between 12 and 1188 m.year^{-1} and the annual average varies significantly from 91 m.year^{-1} (between 2010/2012) to 606 m.year^{-1} (between 2013/2015) (Table 2). The knickpoints identification, and thus migration, is easily followed thanks to the occurrence of typical erosion areas along the axial channel which are restricted downstream by the previous position of a given knickpoint and limited upstream by the current position of the same knickpoint (Figure 5B, D, F, H). These typical erosion areas have no discontinuities (such as little deposit areas inside these erosion areas) and are clearly limited by the two positions in time of a same knickpoints. The position of knickpoints and the position of erosion of deposit areas (bathymetric difference maps) are independently determined, and their superimposition perfectly match. Velocities are 1.45 times higher around bends than in straight sections: the average knickpoints migration in bends is about 354 m.year^{-1} whereas it is about 244 m.year^{-1} in straight sections. In the canyon head, the morphological changes between two successive surveys are too important to draw interpretation on the yearly evolution of knickpoints and CSBs.

Knickpoints upstream migration is characterized by the concomitant migration of areas with erosion (downstream knickpoint) and areas with deposition (upstream knickpoint) (*Figure 5*). This outlines that morphological changes in the channel are dominated by longitudinal retrogressive erosion. The longitudinal channel profile shows evolutions in the form of knickpoints migrations but also of fluctuations of overall carving and infilling (*Figure 6*). The amplitude of fluctuations ranges between -5 m and +20 m relative to the precedent longitudinal profile. Between 2010 and 2018 and after the passage of knickpoints, the longitudinal profiles between the 4 km and 9.5 km section hold the same position, with a relatively smooth and regular ~1° slope. It remains stable over that time period compare to general evolution of the surrounding canyon floor. This suggests that the thalweg has reached a local and transient steady state during this period as a result of a major knickpoint upward migration (Figure 6). On the other hand, on the same section, the 1998 profile (blue line on *Figure 6*) appears significantly far from this 2010-2018 steady state, as it presents a 20 m offset relative to the steady state (*Figure 6*). On this section, the longitudinal profile of the upper canyon reaches a steady state just downstream the knickpoints.

4.2.4. TERRACES

The 2018 DEM shows 9 low-laying and elongated terraces along the canyon (*Figure 3*). The emergence of such terraces is also described in the Monterey canyon (Smith et al., 2005). Interestingly, in both Monterey and Capbreton canyons, the low elevation terraces are located in outer bends with low curvature (*Figure 3*) whereas high curvature outer bends do not exhibit terraces (*Figure 5*).

Terraces show a maximal width of about 140 m, a maximal length of about 1100 m and an elevation above the channel floor that reaches up to 16 m. None of these terraces were present on the 1998 DEM. Their emergence between 1998 and 2010 is related to the deepening of the axial channel and to the gradual lateral erosion of the terraces' flanks (*Figure 7*). This demonstrates the occurrence of at least one gravity flow between 1998 and 2010 strong enough to remove a considerable amount of sediment. Between 2010 and 2018 these terraces experienced a lateral retreat ranging from 30 m (LT6) to 150m (LT9) together with a slight (< 4 m) aggradation. This leads to significantly reshaped terraces (LT4, LT6) and even to the wipe out of LT3 and LT5. Lateral erosion of terraces (especially LT3, LT4 and LT5) is combined with sliding, as evidenced by small coalescent slump scars, and associated to edge mass transport deposits in the channel (zoom on *Figure 3*B).

The retrieval of piston core KS05 in 2013 in addition to the time-lapse bathymetric surveys allows us to present terrace LT4 with considerable details. LT4 cross sections (Figure 7) show significant modifications of the channel floor between 1998 and 2010 with an 8.49 m lateral sediment build-up that resulted in the formation of LT4 and an axial 3.09 m digging leading to a narrower channel. The slope of LT4 increases from 20° in 2010 to 39° in 2018. The lateral erosion ranges from -1.32 $m.year^{-1}$ to -16.25 $m.year^{-1}$ and the aggradation on terraces is comprised between 0.29 $m.year^{-1}$ and 0.40 $m.year^{-1}$, except between 2012 and 2013 where it is null (Table 2). Due to the vertical uncertainties involved, a quantitative study of the aggradation is questionable. A qualitative study of the bathymetric evolution of the terraces remains significant in regard to the trend to aggradation that is clearly identified between each DEM (2010-2018). Between 2010 and 2018, LT4 was gradually reshaped with (1) a total aggradation of about 2 m on top of the terrace, (2) a continuous increase of the slope of the side of the terrace and (3) a gradual lateral erosion in the order of 80 m.

4.2.5. ACCURATE VOLUME QUANTIFICATION

The time-lapse bathymetric survey enabled us to establish the first accurate erosion *vs*. deposit volume quantification on the Capbreton canyon floor based on bathymetric differentials (*Table 3*). The volume budgets in the head and upper canyon have been calculated separately due to their significant different overall morphology. Indeed, features such as CSBs in the head and knickpoints in the upper canyon, along with possibly different hydro-sedimentary processes in the upper canyon, result in alternate positive and negative values for volume budgets calculated from consecutive observations (*Table 3*, *Figure 9*). These values range from -687 681 $m^3.year^{-1}$ (net depletion between 2012 and 2013) to +1 261 542 $m^3.year^{-1}$ (net augmentation between 2015 and 2016) while the minimum budget is -87 952 m^3. $year^{-1}$ (net depletion between 2016 and 2018). These results show that 2010/2012 (638 717 $m^3.year^{-1}$) and 2015/2016 (1 261 542 $m^3.year^{-1}$) are filling periods whereas 1998/2010 (-337 274 $m^3.year^{-1}$), 2012/2013 (-687 681 $m^3.year^{-1}$), 2013/2015 (-455 922 $m^3.year^{-1}$) and 2016/2018 (-87 952 $m^3.year^{-1}$) are erosive periods (*Table 3*). In the canyon head, the yearly sedimentation rate values are in the same order of magnitude of those in the upper canyon. However, in the canyon head the budget is always positive. The maximum sediment accumulation is +722 502 $m^3.year^{-1}$ recorded between 2015 and 2016, and the minimal deposition rate is +16 155 $m^3.year^{-1}$ between 2010 and 2012 (*Table 3*). These volumes are comparable to those of the longshore drift (30 000 to 600 000 $m^3.year^{-1}$; Abadie et al., 2006; Idier et al., 2013). The yearly positive budget in the canyon head since 1998 is not in agreement with the view that the canyon head morphology fluctuated around a stable position of equilibrium, suggesting that the sedimentary budget is null (Mazières et al., 2014). It is also noteworthy that the net sediment gain of the upper canyon combined with that of the head, for the periods 2012/2010 and 2016/2015, can be 3 time greater than the positive longshore drift budget estimated by Idier et al. (2013). This suggests that an additional lateral source from the shelf feeds the upper canyon.

4.3. SEDIMENT CORE ANALYSIS

Core KS05 collected in 2013 on LT4 (Figure 8) presents two lithofacies (U1, U2): U1 consists of an alternance of terrigenous mud and silicoclastic medium sand (250 µm) whereas U2 consists of silicoclastic medium sand (Figure 8). From the bottom of the core to 82 cm, there is a massive deposit, that we assume to be two phases of the same grain flow deposit, considering the rather constant grain size and the few structures as cross-laminations (interpreted as current ripple bedding) observed at 144 cm. The U1 sandy layers are interpreted as grain flows deposited by recurrent low energy gravity flows with a sufficient thickness to bring coarse sediment (sand) on top of these low terraces. Muddy layers are not interpreted as genetically related to the sandy turbidites because of the lack of gradual contact. The smear slides collected in U1 reveal that the mud contains rare foraminifera but few carbonate bioclasts such as red algae, echinoderms or bryozoans; which have been observed on the canyon flanks by ROV during the cruise HaPoGé (Gillet and De Casamajor, 2017). Carbonate bioclasts are the most abundant and largest between 68-82 cm at the base of U1. This suggests terrigenous-dominated sedimentation with a low pelagic contribution with some shelf bioclastic and contributions from the canyon flanks. The probable sources are the Adour River plume (Petus et al., 2014) and reworked sediments of the Basque continental shelf mud patch (Jouanneau et al., 2008). $^{210}Pb_{xs}$ was used to add temporal constraints on the sediment accumulation. At the top of the core, $^{210}Pb_{xs}$ presents a low activity (15±4 mBq g^{-1}) associated with low ^{232}Th (19±1 mBq g^{-1}), that is explained by the sandy nature of the sediment (Figure 8). In depth, between 24 and 72 cm, $^{210}Pb_{xs}$ and ^{232}Th measured in the muddy layers present rather constant activities (127-137 and 27-30 mBq g^{-1}, respectively). This allows us to interpret that this sediment section has been deposited during a short time interval (< ~1 years). Between 71 cm and the top of the deep sandy layer (U2), $^{210}Pb_{xs}$ presents a fast decrease. The deepest measured $^{210}Pb_{xs}$, although sampled with care, is clearly diluted by sand (^{232}Th of 16±1 mBq g^{-1}) and is not suitable for chronology. Only the decrease of $^{210}Pb_{xs}$ activities between 71 and 79 could then be used to estimate a mean maximum sedimentation accumulation rate of about 0.19 cm $year^{-1}$. Although this estimate is rather approximate, it indicates that background sedimentation is low compared to the considerable contributions of grain flow deposits.

5. DISCUSSION

5.1. RETROGRESSIVE EROSION EVIDENCED BY UPSTREAM MIGRATION OF KNICKPOINTS

Successive bathymetric surveys between 1998 and 2018, reveal that the Capbreton canyon floor morphology changed significantly over the 20 years covered. Changes are outlined by areas of sediment accumulation and depletion dominantly driven by retrogressive erosion in the form of upstream migration of knickpoints on the axial channel floor.

Turbidity currents form upstream migrating cyclic steps when the flow passes from a subcritical flow on the stoss side of a step to a supercritical flow on the lee side, through the formation of a hydraulic jump. The flow conditions changing from subcritical, to supercritical conditions, passing through a critical point (i.e., densimetric Froude=1) then returning back to a subcritical regime downstream from the hydraulic jump. In terms of morphology, these hydrodynamic conditions can lead to downslope or upslope asymmetrical cyclic bedforms both migrating upslope (Parker 1996, Cartigny et al., 2011).

The CSBs in the head of the Capbreton canyon are asymmetrical downslope bedforms. The important morphological changes affecting these features in the canyon head between two successive surveys suggest that they are probably subject to migration. However, the bathymetric time-lapse do not clearly evidence an upstream migration. The series of CSBs observed are interpreted as cyclic steps. On the contrary, it would be difficult to assimilate all the knickpoints in the canyon to a unique series of cyclic steps due to the irregularity of their distribution and therefore their lack of cyclicity. Nevertheless, within a group of several coalescent knickpoints (from 2 to 6), similar processes (high variability of flow conditions including hydraulic jumps) may be involved and the terminology of cyclic steps can be considered.

To understand the evolution of bedforms (CSBs and knickpoints), two high-resolution bathymetric surveys were recorded within a 4-days interval in June 2012 (SEDYMAQ3 cruise; Gillet, 2012). No movements were observed suggesting that no event of sufficient energy to affect the canyon floor occurred. This indicates that processes with reoccurrences of less than 4 days such as internal tides or internal waves have no potential role in shaping or reshaping the features observed in the Capbreton canyon. The study of Paull et al. (2011) based on 2 high-resolution bathymetric surveys recorded within a 24-hours interval in the Monterey canyon led the authors to the same conclusion. Feature migration in both locations (i.e. Capbreton canyon and Monterey canyon) are thus linked to exceptional events such as exceptional swell, storms or sedimentary destabilization with no external trigger. The unit in which we express the velocity of knickpoint migrations (12 m.year^{-1} to 1188 m.year^{-1}) in meters per year, but laboratory experiments suggest that the migration of knickpoints occurs in fact over short periods of time corresponding to the duration of the transit of one or several turbidity currents.

The generation of knickpoints and their migration may be related to turbiditic events, and in fact analogic experiments showed that one turbidity current can generate knickpoints (Toniolo and Cantelli, 2007). Previous laboratory experiments on non-indurated sediments (simulating river alluvial beds) demonstrated that, under Froude-supercritical flow conditions, an instantaneous drop in base level can lead to the formation of upstream-migrating knickpoints (Cantelli and Muto, 2014). A single base-level fall can generate a single knickpoint, or multiple knickpoints that lead to a new equilibrium profile. The longitudinal profile of the uppermost part of the Capbreton canyon (*Figure 6*) is similar to the observations made by Cantelli and Muto (2014): the consequence of the upstream-migrating knickpoints, through the different DEMs, is the establishment of a new local steady state along the canyon axis as far as knickpoints are migrating. We may suggest that the canyon longitudinal profile tends to reach a local and transient equilibrium profile. Different studies (Gerber et al., 2009; Tubau et al., 2015) have described an equilibrium profile in canyons, but they state of an overall profile. In our study, the upper part of the Capbreton canyon seems to reach a very local and transient equilibrium profile. Taking into consideration the study area (9.5 km over 300 km) and the time period studied, this study cannot claim to establish the trend of the overall profile and cannot pretending either that the processes described here are applicable to the entire canyon and over the past. The locale and transient equilibrium profile is shaped by minor processes and results from the type of flows. This equilibrium profile results from hydrodynamic balancing without depending on depth as described in continental concepts.

On figure 6, from 4 km to 9.5 km downstream the head, the position of the local and transient equilibrium profile is based on our observations. The corresponding curve has been established by a simple mean of long profiles extract from DEMs from 2010 to 2018 and from 4 to 9.5 km downstream the head. To draw the possible upward extension of this curve and represent the position of a supposed local equilibrium profile between the observed steady state (downstream the knickpoints) and the canyon head (from 4 km to the head), a simple power law averaged over the 7 DEMs available from years 1998 to 2018 was used. The migration of knickpoints and the generation of new knickpoints observed between each bathymetric survey is a new demonstration of the canyon activity. The one-year period between the 2012 and 2013 surveys, and the 2015 and 2016 surveys suggest that turbiditic events may occur as often as once a year in the Capbreton Canyon. This is in accordance with the results of Brocheray et al. (2014) downstream the canyon (for the last 2000 years).

5.2. TERRACES EVOLUTION IN THE UPPER PART OF THE CANYON

Between 2010 and 2018, the reshaping of low terraces is observed in the form of (1) aggradation, (2) lateral retrogressive erosion correlated to channel widening, and (3) increase of lateral slope. However, the magnitude of this evolution is not constant and the most important modifications were observed between 1998 and 2010 (*Figure 7*). There were nearly no terraces between 1998 and 2010 and their emergence started in 2010 with the inception of an axial channel digging along the canyon floor. This is supported by the alignment of the top of LT3, LT4, LT5, LT6 and LT7 along a rectilinear on a constant slope (1°) profile suggesting that the top of the terraces was actually the canyon floor before 2010 (*Figure 7*, *Figure 10*).

Sediment core KS05 was retrieved in 2013 on the flank of LT4. The 2015 survey demonstrated notable morphological differences with the 2013 DEM, with a significant lateral retrogressive erosion of LT4, and indicates that the entire thickness of core KS05 (2.10 m) was eroded between 2013 and 2015. The lithofacies at the base of core KS05 shows that the axial channel was created by the erosion of medium sand as seen in unit 2. Unit 1, characterized by interbedded sandy and muddy layers, may correspond to turbiditic spillover deposits intercalated with nepheloid settling deposits on top of the terrace before 2013 (*Figure 7*C). These turbiditic events are likely involved in the aggradation process still taking place on the remaining terraces. $^{210}Pb_{xs}$ activity indicates that the sediment from 80 cm to the top of the core was likely deposited in a short period of time, probably less than 1 year. The low pelagic biogenic content of the muddy intervals suggests a hemipelagic sedimentation (terrigenous dominated) with a source from the Adour plume. The Adour River must thus have a significant role in the canyon supply. The grain size in unit 2 (i.e. medium sand with a median around 250 µm) is similar to that in the canyon head and on the Aquitain longshore drift (Mazières et al., 2014).

A conceptual model describing the emergence of low elevation terraces can be drawn (*Figure 11*). Phase 1 corresponds to the partial filling of the canyon due to grain flow deposits in several steps. During phase 2, the thalweg is incised and leads to terrace formation by vertical and lateral erosion, combined to aggradation of spillover deposits characterized by low energy turbiditic events and hemipelagic deposits. During phase 3, the incised channel reaches a local and transient equilibrium profile, vertical erosion and channel deepening locally cease, but terraces are still being shaped by lateral erosion of the channel and aggradation of deposits from low energy turbiditic events and by hemipelagic deposits; the lateral slope increases. In phase 4, the terrace is only shaped by lateral erosion, which increases the lateral slope, and by aggradation.

The low elevation terraces described here are interpreted as short-lived features similar to those observed in the Monterey canyon (Smith et al., 2005), the difference being that the Capbreton terrace cycle takes place over a decade, as opposed to sub-annually as observed in the Monterey canyon.

5.3. PROCESSES OF CANYON TRANSIENT MORPHOLGY

Pioneering work on the upper part of the Capbreton canyon, based on canyon head longitudinal profiles, concluded that the head fluctuates around a stable position of equilibrium (Mazières et al.,2014). The new volume quantification of sediments on the Capbreton canyon floor from this work shows that, between consecutive years, sediment budget in the upper canyon is a succession of filling and erosive periods, whereas the sediment budget in the head was consistently positive during the last 20 years. Such results confirm that the head of Capbreton canyon traps sand and mud before discharging the sediment toward the upper canyon. Our findings thus question the notion that the Capbreton canyon is a sediment buffer on an annual time scale.

The volume budget between 1998 and 2018 is negative. The upper part of the Capbreton Canyon is dominated by erosive processes. Care was taken in our study to express all volumes by surface units to give metric accumulation or depletion rates (*Table 3*). The sedimentation rates in the head have the same order of magnitude as those in the canyon. Along with the canyon flanks inactivity, this demonstrates that the head is the main sediment source.

One of the most important points issued from the analysis of this bathymetric time series is that, in the study area, the canyon floor morphology of 1998 differs completely from the morphology observed thereafter. During the short 20-year period, the Capbreton canyon seems to have two distinct mode which can be observed in the very upper part: (1) a mode in which the thalweg is flat and the sedimentary stock is above the local equilibrium profile (*Figure 11*A); and (2) a mode characterised by an axial channel incision associated to residual terraces when the canyon is reaching this local equilibrium profile (*Figure 11*B and C).

Mode 1 (*Figure 12*A) was observed in 1998, and possibly occurred sometime between 1998 and 2010 (*Figure 10*). The longitudinal profile was above the local equilibrium profile all along the upper part of the canyon. This sediment stock could have been established during a long time period and/or more probably in high quantities during a unique or few gravity events. The description of this mode is limited due to the lack of DEM before 1998 and between 1998 and 2010.

Mode 2 (*Figure 12*B) has occurred at least since 2010. The description of this second mode is based on 6 DEM recovered in 8 years. Mode 2 consists of a dynamic evolution of the canyon reaches a new and local equilibrium profile through the deepening of an axial channel associated to residual elevation of the lateral terraces. The retrogressive erosion, evidenced by knickpoints, starts downstream the canyon and progresses through the years toward the canyon head. The thalweg deepening toward the equilibrium profile is gradual, and is driven by upstream-migrating knickpoints. As knickpoints progress, the longitudinal profile gets closer to the local equilibrium profile (*Figure 12*B).

We propose that mode 1 (before 1998 and sometime before 2010; *Figure 11*A) is characterised by the occurrence of punctual, high-energy events, whereas mode 2 mostly consists of recurrent, low energy events and is dominated by erosional processes. The switch from one mode to the other may have been triggered by an exceptional gravity event, such as the one associated to storm Martin in 1999 (Mulder et al., 2001). This extreme, punctual event was likely to have induced a flush of sediment previously stored in the head toward the upper canyon, which would be expected to fill the thalweg and produce a flat floor morphology such as that observed in 1998 (mode 1).The absence of DEMs in the years immediately following storm Martin makes it impossible for us to confirm whether the transition from mode 1 to state 2 was effectively triggered by this event. Our findings raise questions regarding the cyclicity of the shifts between the two modes, which, hypothetically, can be due to internal dynamics of the canyon. Due to the lack of DEMs before 1998, we cannot assess any possible long-term alternation of these two modes, nor the filling of previous axial channel.

Furthermore, the rare “high” temporal resolution of our dataset enabled us to characterise the dynamics of the Capbreton canyon over a period of 20 years, but the absence of sub-annual surveys prevented us to identify any seasonal effect on the evolution of the canyon morphology.

6. CONCLUSION

We present a rather rare morphobathymetric time lapse survey of the Capbreton canyon head and upper canyon between 1998 and 2018 to investigate their morphological evolution on a multi-annual basis. Subtraction of repeated DEMs gives volumetric information on sedimentary transport, erosion and deposit from which the main conclusions are:

(1) The main feature in the morphological evolution of the Capbreton canyon is the incision of an axial channel mainly driven by knickpoint's regression and the digging of residual terraces in the upper canyon since 2010. The overall morphology and location of the canyon's upper part remained the same.

(2) Between 2010 and 2018, the channel incision in the upper canyon was accompanied by the development of along-channel, elongated, low elevation terraces, and by upstream migrating knickpoints. Terraces are reshaped by lateral erosion from channel widening and by aggradation of turbiditic spillover deposits, as well as hemipelagic deposits. Knickpoint upstream migration can reach up to 1180 m/year but fluctuates spatially and temporally.

(3) Over the last 20 years (1998 to 2018), two morphological modes were observed in the upper part of Capbreton canyon, each linked to distinct dynamical processes: (1) relative flat canyon floor (only observed in 1998) resulting from a local filling excess of the thalweg, and (2) the canyon transiently reaches a local equilibrium profile through the digging of an axial channel by upstream-migrating knickpoints leaving residual low lateral terraces.

(4) The canyon head and upper canyon are characterized both by areas of accumulation and depletion. The volumetric budget shows that the canyon head recorded accumulations of 1.9 Mm^3 (0.11 Mm^3/year) between 2001 and 2016, while the upper canyon demonstrated depletions of 4.2 Mm3 (0.24 Mm^3/year) between 1998 and 2018. However, the canyon underwent only two periods of accumulation, while the canyon head was constantly subjected to accumulation.

(5) The contrasted morphologies and volumetric budgets between the head and the upper canyon outline the different sedimentary processes affecting the canyon, and suggest that the canyon head acts as an important sediment buffer, the potential of which is still unknown.

(6) Sediment buffering in the canyon head is possibly the pace maker of the canyon's sedimentary dynamics, with alternating periods of accumulation in the canyon head and depletion in the canyon, followed by the flushing of sediment from the canyon head and accumulation in the canyon. The potential cyclic character of periods of accumulation and flushing remains speculative. They may be driven by internal forcing such as the canyon intrinsic storage capacity and/or by external forcing such as extreme storms.

(7) The buffering capacity of the canyon head infers a delayed transfer of sediment from source to sink, at least on a pluriannual time scale. Though it may not be perceptible in the geological record in terms of volumes, it must however control the nature of gravity flows involved in the sediment transfer and therefore the structure and composition of deposits in the sink.

(8) . The volume quantification and core sedimentology analysis also prove that there is a lateral supply from the plateau and the Adour River plume, probably through active gullies.

The temporal resolution of the repeated DEMs in this study does not provide insight into any seasonal morphological fluctuations of the canyon. Further annual or semi-annual bathymetric surveys are needed to fully encompass the potential cyclicity in the sediment transfer from the canyon head into the upper canyon.

7. ACKNOWLEDGMENTS

IFREMER, the Flotte Océanique Française and all the crews of the R/V La Thalia and Le Suroît are thanked for their assistance during cruises ITSAS I (Cirac, 1998), ITSAS V (Cirac, 2001), SEDYMAQ 2 (Gillet, 2010), SEDYMAQ 3 (Gillet, 2012), SEDYMAQ 4 (Gillet, 2018), VOLT 1 (Simplet, 2015), VOLT 2 (Silva Jacinto, 2016). We thank the Marine Nationale (French Navy), the SHOM and especially Thierry

Garlan to have provided the DEM and core KS05 acquired during cruise PROTEUS-DUNES 2013 (Mathias, 2013) on the R/V Beautemps-Beaupré. Michel Cremer, Emmanuelle Ducassou, Sébastien Zaragosi and the sedimentology technical staff of EPOC are thanked for the realization and the interpretation of the grain size analysis and RX on core KS05. We thank Jeffrey Peakall for fruitful discussions, and Eleanor Georgiadis for the English corrections. Our gratitude is also extended to RTE for having chartered the vessels for the VOLT 1 and VOLT 2 cruises and for having granted us permission to use the data.

Abadie, S., Butel, R., Mauriet, S., Morichon, D., Dupuis, H., 2006. Wave climate and longshore drift on the South Aquitaine coast. Cont. Shelf Res. 26, 1924–1939. https://doi.org/10.1016/j.csr.2006.06.005

Antonov, J. I., D. Seidov, T. P. Boyer, R. A. Locarnini, A. V. Mishonov, H. E. Garcia, O. K. Baranova, M. M. Zweng, and D. R. Johnson, 2010. World Ocean Atlas 2009, Volume 2: Salinity. S. Levitus, Ed. NOAA Atlas NESDIS 69, U.S. Government Printing Office, Washington, D.C., 184 pp.

Azpiroz-Zabala, Maria, Cartigny, Matthieu J B, Talling, Peter J, Parsons, Daniel R, Sumner, Esther J, Clare, Michael A, . . . Pope, Ed L. (2017). Newly recognized turbidity current structure can explain prolonged flushing of submarine canyons. Science Advances., 3(10), E1700200. https://doi.org/10.1126/sciadv.1700200

Babonneau, N., Savoye, B., Cremer, M., Bez, M., 2010. Sedimentary Architecture in Meanders of a Submarine Channel: Detailed Study of the Present Congo Turbidite Channel (Zaiango Project). J. Sediment. Res. 80, 852–866. https://doi.org/10.2110/jsr.2010.078

Babonneau, N., Savoye, B., Cremer, M., Bez, M., 2004. Multiple terraces within the deep incised Zaire Valley (ZaïAngo Project): are they confined levees? Geol. Soc. Lond. Spec. Publ. 222, 91–114. https://doi.org/10.1144/GSL.SP.2004.222.01.06

Babonneau, N., Savoye, B., Cremer, M., Bez, M., 2002. Processes and Sedimentary Architectures along the Present Zaire Turbidite Channel (ZAIANGO project). AAPG Annu. Meet. Abstract A11.

Batifoulier, F., Lazure, P., Bonneton, P., 2012. Poleward coastal jets induced by westerlies in the Bay of Biscay. J. Geophys. Res. Oceans 117, n/a-n/a. https://doi.org/10.1029/2011JC007658

Bois, C., Pinet, B., Gariel, O., 1997. The sedimentary cover along the ECORS Bay of Biscay deep seismic reflection profile. A comparison between the Parentis basin and other European rifts and basins. Mém. Société Géologique Fr. 171, 143–165.

Boyer, T.P., J. I. Antonov, O. K. Baranova, C. Coleman, H. E. Garcia, A. Grodsky, D. R. Johnson, R. A. Locarnini, A. V. Mishonov, T.D. O'Brien, C.R. Paver, J.R. Reagan, D. Seidov, I. V. Smolyar, and M. M. Zweng, 2013: World Ocean Database 2013, NOAA Atlas NESDIS 72, S. Levitus, Ed., A. Mishonov, Technical Ed.; Silver Spring, MD, 209 pp., http://doi.org/10.7289/V5NZ85MT

Brocheray, S., Cremer, M., Zaragosi, S., Schmidt, S., Eynaud, F., Rossignol, L., Gillet, H., 2014. 2000years of frequent turbidite activity in the Capbreton Canyon (Bay of Biscay). Mar. Geol. 347, 136–152. https://doi.org/10.1016/j.margeo.2013.11.009

Cantelli, A., Muto, T., 2014. Multiple knickpoints in an alluvial river generated by a single instantaneous drop in base level: experimental investigation. Earth Surf. Dyn. 2, 271–278. https://doi.org/10.5194/esurf-2-271-2014

Cartigny, M.J.B., Postma, G., van den Berg, J.H., Mastbergen, D.R., 2011. A comparative study of sediment waves and cyclic steps based on geometries, internal structures and numerical modeling. Mar. Geol. 280, 40–56. https://doi.org/10.1016/j.margeo.2010.11.006

CASAGEC Ingénierie, 2016. Transfert hydraulique de sédiments marins pour le rechargement annuel des plages sud de Capbreton.

Cirac, P., 2001. ITSAS V Cruise. RV Le Suroît. https://doi.org/10.17600/1070060

Cirac, P., 1998. ITSAS Cruise. RV Thalia. https://doi.org/10.17600/98020070

Cirac, P., Bourillet, J.-F., Griboulard, R., Normand, A., 2001. Le canyon de Capbreton : nouvelles approches morphostructurales et morphosédimentaires. Premiers résultats de la campagne Itsas. Comptes Rendus Académie Sci. - Ser. IIA - Earth Planet. Sci. 332, 447–455. https://doi.org/10.1016/S1251-8050(01)01557-9

Clarke J.E.H., Marques C.R.V., Pratomo D. (2014) Imaging Active Mass-Wasting and Sediment Flows on a Fjord Delta, Squamish, British Columbia. In: Krastel S. et al. (eds) Submarine Mass Movements and Their Consequences. Advances in Natural and Technological Hazards Research, vol 37. Springer, Cham. https://doi.org/10.1007/978-3-319-00972-8_22

Conway, K.W., Barrie, J.V., Picard, K., Bornhold, B.D., 2012. Submarine channel evolution: active channels in fjords, British Columbia, Canada. Geo-Mar. Lett. 32, 301–312. https://doi.org/10.1007/s00367-012-0280-4

Cremer, M., 1983. Approches sédimentologique et géophysique des accumulations turbiditiques: l'éventail profond du Cap-Ferret (Golfe de Gascogne), la série des grès d'Annot (Alpes-de-Haute-Provence) 213.

Deregnaucourt, D., Boillot, G., 1982. Nouvelle carte structurale du golfe de Gascogne. Comptes Rendus Académie Sci. Paris Serie II 294, 219–222.

Durrieu de Madron, X., 1994. Hydrography and nepheloid structures in the Grand-Rhône canyon. Cont. Shelf Res. 14, 457–477. https://doi.org/10.1016/0278-4343(94)90098-1

Ferrer, O., Roca, E., Benjumea, B., Muñoz, J.A., Ellouz, N., MARCONI Team, 2008. The deep seismic reflection MARCONI-3 profile: Role of extensional Mesozoic structure during the Pyrenean contractional deformation at the eastern part of the Bay of Biscay. Mar. Pet. Geol. 25, 714–730. https://doi.org/10.1016/j.marpetgeo.2008.06.002

Froidefond, J., Castaing, P., Weber, O., 1983. Evolution morpho-sedimentaire de la tete du Canyon de Capbreton d'apres les cartes de 1860 a 1963, utilisation des methodes informatiques. Bull. Société Géologique Fr. 7, 705–714.

Froidefond, J.M., 1982. Processus d'évolution d'un littoral sableux aux cours de l'holocène. Application au domaine aquitain. Présentation d'une méthode de géomorphologie dynamique et quantitative. University of Bordeaux 1, France.

Gaudin, M., Mulder, T., Cirac, P., Berné, S., Imbert, P., 2006. Past and present sedimentary activity in the Capbreton Canyon, southern Bay of Biscay. Geo-Mar. Lett. 26, 331–345. https://doi.org/10.1007/s00367-006-0043-1

Gerber, T.P., Amblas, D., Wolinsky, M.A., Pratson, L.F., Canals, M., 2009. A model for the long-profile shape of submarine canyons. J. Geophys. Res. 114, F03002. https://doi.org/10.1029/2008JF001190

Gillet, H., 2018. SEDYMAQ4 Cruise. RV Thalia. https://doi.org/10.17600/18000424

Gillet, H., 2012. SEDYMAQ3 Cruise. RV Thalia. https://doi.org/10.17600/12070080

Gillet, H., 2010. SEDYMAQ2 Cruise. RV Thalia. https://doi.org/10.17600/10070100

Gillet, H., De Casamajor, M.-N., 2017. HAPOGE Cruise. RV Côtes De La Manche. https://doi.org/10.17600/17010700

Gillet, H., Guiastrennec-Faugas, L., Gazzoli, L., 2019. ROV submarine exploration of the proximal part of the Capbreton canyon (Bay of Biscay). Morphological surprises and discovery of cold seep-related authigenic carbonate structures. EGU Gen. Assem. 2019 21, 1.

Hage, S., Cartigny, M.J.B., Clare, M.A., Sumner, E.J., Vendettuoli, D., Hughes Clarke, J.E., Hubbard, S.M., Talling, P.J., Lintern, D.G., Stacey, C.D., Englert, R.G., Vardy, M.E., Hunt, J.E., Yokokawa, M., Parsons, D.R., Hizzett, J.L., Azpiroz-Zabala, M., Vellinga, A.J., 2018. How to recognize crescentic bedforms formed by supercritical turbidity currents in the geologic record: Insights from active submarine channels. Geology 46, 563–566. https://doi.org/10.1130/G40095.1

Harris, P.T., Whiteway, T., 2011. Global distribution of large submarine canyons: Geomorphic differences between active and passive continental margins. Mar. Geol. 285, 69–86. https://doi.org/10.1016/j.margeo.2011.05.008

Hay, A.E., 1987. Turbidity currents and submarine channel formation in Rupert Inlet, British Columbia: 2. The roles of continuous and surge-type flow. J. Geophys. Res. 92, 2883. https://doi.org/10.1029/JC092iC03p02883

Idier, D., Castelle, B., Charles, E., Mallet, C., 2013. Longshore sediment flux hindcast: spatio-temporal variability along the SW Atlantic coast of France. J. Coast. Res. 165, 1785–1790. https://doi.org/10.2112/SI65-302.1

Jouanneau, J.-M., Weber, O., Champilou, N., Cirac, P., Muxika, I., Borja, A., Pascual, A., Rodríguez-Lázaro, J., Donard, O., 2008. Recent sedimentary study of the shelf of the Basque country. J. Mar. Syst. 72, 397–406. https://doi.org/10.1016/j.jmarsys.2007.03.013

Kelner, M., Migeon, S., Tric, E., Couboulex, F., Dano, A., Lebourg, T., Taboada, A., 2016. Frequency and triggering of small-scale submarine landslides on decadal timescales: Analysis of 4D bathymetric data from the continental slope offshore Nice (France). Mar. Geol. 379, 281–297. https://doi.org/10.1016/j.margeo.2016.06.009

Khripounoff, A., Crassous, P., Lo Bue, N., Dennielou, B., Silva Jacinto, R., 2012. Different types of sediment gravity flows detected in the Var submarine canyon (northwestern Mediterranean Sea). Prog. Oceanogr. 106, 138–153. https://doi.org/10.1016/j.pocean.2012.09.001

Khripounoff, A., Vangriesheim, A., Babonneau, N., Crassous, P., Dennielou, B., Savoye, B., 2003. Direct observation of intense turbidity current activity in the Zaire submarine valley at 4000 m water depth. Mar. Geol. 194, 151–158. https://doi.org/10.1016/S0025-3227(02)00677-1

Klingebiel, A., Legigan, P., 1978. Histoire géologique des divagations de l’Adour Proc Congr IVème Centenaire du Détournement de l’Adour 1578–1978, Bayonne.

Kolodziejczyk Nicolas, Prigent-Mazella Annaig, Gaillard Fabienne (2017). ISAS-15 temperature and salinity gridded fields. SEANOE. https://doi.org/10.17882/52367

Lintern, D.G., Hill, P.R., Stacey, C., 2016. Powerful unconfined turbidity current captured by cabled observatory on the Fraser River delta slope, British Columbia, Canada. Sedimentology 63, 1041–1064. https://doi.org/10.1111/sed.12262

Locarnini, R. A., A. V. Mishonov, J. I. Antonov, T. P. Boyer, H. E. Garcia, O. K. Baranova, M. M. Zweng, and D. R. Johnson, 2010. World Ocean Atlas 2009, Volume 1: Temperature. S. Levitus, Ed. NOAA Atlas NESDIS 68, U.S. Government Printing Office, Washington, D.C., 184 pp.

Maier, K.L., Johnson, S.Y., Hart, P., 2018. Controls on submarine canyon head evolution: Monterey Canyon, offshore central California. Mar. Geol. 404, 24–40. https://doi.org/10.1016/j.margeo.2018.06.014

Mary, Y., Eynaud, F., Zaragosi, S., Malaizé, B., Cremer, M., Schmidt, S., 2015. High frequency environmental changes and deposition processes in a 2 kyr-long sedimentological record from the Cap-Breton canyon (Bay of Biscay). The Holocene 25, 348–365. https://doi.org/10.1177/0959683614558647

Mathias, X., 2013. PROTEUS DUNES 2013 Cruise. RV Beautemps Beaupré. http://dx.doi.org/10.17183/LOTS_BATHY#S201306500-09. http://dx.doi.org/10.17183/LOTS_BATHY#S201306500-11.

Mazières, A., Gillet, H., Castelle, B., Mulder, T., Guyot, C., Garlan, T., Mallet, C., 2014. High-resolution morphobathymetric analysis and evolution of Capbreton submarine canyon head (Southeast Bay of Biscay—French Atlantic Coast) over the last decade using descriptive and numerical modeling. Mar. Geol. 351, 1–12. https://doi.org/10.1016/j.margeo.2014.03.001

Migeon, S., Mulder, T., Savoye, B., Sage, F., 2006. The Var turbidite system (Ligurian Sea, northwestern Mediterranean)—morphology, sediment supply, construction of turbidite levee and sediment waves: implications for hydrocarbon reservoirs. Geo-Mar. Lett. 26, 361–371. https://doi.org/10.1007/s00367-006-0047-x

Mulder, T., Gillet, H., Hanquiez, V., Ducassou, E., Fauquembergue, K., Principaud, M., Conesa, G., Le Goff, J., Ragusa, J., Bashah, S., Bujan, S., Reijmer, J., Cavailhes, T., Droxler, A., Blank, D., Guiastrennec, L., Fabregas, N., Recouvreur, A., Seibert, C., 2017. Carbonate slope morphology revealing a giant submarine canyon (Little Bahama Bank, Bahamas). Geology.

Mulder, T., Weber, O., Anschutz, P., Jorissen, F., Jouanneau, J.-M., 2001. A few months-old storm-generated turbidite deposited in the Capbreton Canyon (Bay of Biscay, SW France). Geo-Mar. Lett. 21, 149–156. https://doi.org/10.1007/s003670100077

Mulder, T., Zaragosi, S., Garlan, T., Mavel, J., Cremer, M., Sottolichio, A., Sénéchal, N., Schmidt, S., 2012. Present deep-submarine canyons activity in the Bay of Biscay (NE Atlantic). Mar. Geol. 295–298, 113–127. https://doi.org/10.1016/j.margeo.2011.12.005

Mullenbach, B.L., Nittrouer, C.A., 2000. Rapid deposition of fluvial sediment in the Eel Canyon, northern California. Cont. Shelf Res. 20, 2191–2212. https://doi.org/10.1016/S0278-4343(00)00067-4

Nesteroff, W.D., Heezen, R.C., 1962. Essai de comparaison entre les turbidites modernes et le flysch. Rev. Géogr. phys. et Géol. dyn. 5, 2, 115–127.

Normandeau, A., Lajeunesse, P., St-Onge, G., Bourgault, D., Drouin, S.S.-O., Senneville, S., Bélanger, S., 2014. Morphodynamics in sediment-starved inner-shelf submarine canyons (Lower St.

Lawrence Estuary, Eastern Canada). Mar. Geol. 357, 243–255. https://doi.org/10.1016/j.margeo.2014.08.012

Paull, C. (2002). Caught in the act: The 20 December 2001 gravity flow event in Monterey Canyon. Geo-marine Letters, 22(4), 227-232.

Paull, C.K., Mitts, P., Ussler III, W., Keaten, R., Greene, H.G., 2005. Trail of sand in upper Monterey Canyon: offshore California. Geol. Soc. Am. Bull. 117, 1134–1145. https://doi.org/10.1130/B25390.1.

Paull, C.K., Ussler III, W., Caress, D.W., Lundsten, E., Covault, J.A., Maier, K.L., Xu, J., Augenstein, S., 2010. Origins of large crescent-shaped bedforms within the axial channel of Monterey Canyon, offshore California. Geosphere 6, 1–20. https://doi.org/10.1130/GES00527.1.

Paull, C.K., Caress, D.W., Iii, W.U., Lundsten, E., Meiner-Johnson, M., 2011. High-resolution bathymetry of the axial channels within Monterey and Soquel submarine canyons, offshore central California 25. https://doi.org/10.1130/GES00636.1

Petus, C., 2009. Qualité des eaux côtières du sud du golfe de Gascogne par télédétection spatiale : Méthodologie de détermination et de quantification de substances particulaires et dissoutes. Univ. Bordx. 1 (PhD Thesis).

Petus, C., Marieu, V., Novoa, S., Chust, G., Bruneau, N., Froidefond, J.-M., 2014. Monitoring spatio-temporal variability of the Adour River turbid plume (Bay of Biscay, France) with MODIS 250-m imagery. Cont. Shelf Res. 74, 35–49. https://doi.org/10.1016/j.csr.2013.11.011

Pingree, R.D., Mardell, G.T., New, A.L., 1986. Propagation of internal tides from the upper slopes of the Bay of Biscay. Nature 321, 154.

Pratson, L.F., Ryan, W.B.F., Mountain, G.S., Twichell, D.C., 1994. Submarine canyon initiation by downslope-eroding sediment flows: evidence in late Cenozoic strata on the New Jersey continental slope. Geol. Soc. Am. Bull. 106, 395–412. https://doi.org/10.1130/0016-7606(1994)106<0395:SCIBDE>2.3.CO;2

Puig, P., Palanques, A., Orange, D.L., Lastras, G., Canals, M., 2008. Dense shelf water cascades and sedimentary furrow formation in the Cap de Creus Canyon, northwestern Mediterranean Sea. Cont. Shelf Res. 28, 2017–2030. https://doi.org/10.1016/j.csr.2008.05.002

Salles, T., Mulder, T., Gaudin, M., Cacas, M.C., Lopez, S., Cirac, P., 2008. Simulating the 1999 Capbreton canyon turbidity current with a Cellular Automata model. Geomorphology 97, 516–537. https://doi.org/10.1016/j.geomorph.2007.09.005

Schmidt S., Howa H., Diallo A., Martín J., Cremer M., Duros P., Fontanier Ch., Deflandre B., Metzger E. & Mulder Th. (2014) Recent sediment transport and deposition in the Cap-Ferret Canyon, South-East margin of Bay of Biscay. Deep Sea Research II 104, 134-144. https://doi.org/10.1016/j.dsr2.2013.06.004

Shepard, F.P., 1981. Submarine canyons: multiple causes and long-time persistence. Am. Assoc. Pet. Geol. Bull. 65, 1062–1077.

Shepard, F.P., Dill, R.F., 1966. Submarine Canyon and Others Sea Valleys.

Silva Jacinto, R., 2016. VOLT2 Cruise. RV Thalassa. https://doi.org/10.17600/16006800

Simplet, L., 2015. VOLT1 Cruise. RV Thalia. https://doi.org/10.17600/15003900

Smith, D.P., Kvitek, R., Iampietro, P.J., Wong, K., 2007. Twenty-nine months of geomorphic change in upper Monterey Canyon (2002–2005). Mar. Geol. 236, 79–94. https://doi.org/10.1016/j.margeo.2006.09.024

Smith, D.P., Ruiz, G., Kvitek, R., Iampietro, P.J., 2005. Semiannual patterns of erosion and deposition in upper Monterey Canyon from serial multibeam bathymetry. Geol. Soc. Am. Bull. 117, 1123. https://doi.org/10.1130/B25510.1

Sultan, N., Gaudin, M., Berne, S., Canals, M., Urgeles, R., Lafuerza, S., 2007. Analysis of slope failures in submarine canyon heads: An example from the Gulf of Lions. J. Geophys. Res. 112, F01009. https://doi.org/10.1029/2005JF000408

Talling, P.J., 2014. On the triggers, resulting flow types and frequencies of subaqueous sediment density flows in different settings. Mar. Geol. 352, 155–182. https://doi.org/10.1016/j.margeo.2014.02.006

Toniolo, H., Cantelli, A., 2007. Experiments on Upstream-Migrating Submarine Knickpoints. J. Sediment. Res. 77, 772–783. https://doi.org/10.2110/jsr.2007.067
Tubau, X., Paull, C.K., Lastras, G., Caress, D.W., Canals, M., Lundsten, E., Anderson, K., Gwiazda, R., Amblas, D., 2015. Submarine canyons of Santa Monica Bay, Southern California: Variability in morphology and sedimentary processes. Mar. Geol. 365, 61–79. https://doi.org/10.1016/j.margeo.2015.04.004
Xu, J.P., Noble, M., Eittreim, S.L., Rosenfeld, L.K., Schwing, F.B., Pilskaln, C.H., 2002. Distribution and transport of suspended particulate matter in Monterey Canyon, California. Mar. Geol. 181, 215–234. https://doi.org/10.1016/S0025-3227(01)00268-7
Xu, J.P., Wong, F.L., Kvitek, R., Smith, D.P., Paull, C.K., 2008. Sandwave migration in Monterey Submarine Canyon, Central California. Mar. Geol. 248, 193–212. https://doi.org/10.1016/j.margeo.2007.11.005
Yin, S., Lin, L., Pope, E.L., Li, J., Ding, Weifeng, Wu, Z., Ding, Weiwei, Gao, J., Zhao, D., 2019. Continental slope-confined canyons in the Pearl River Mouth Basin in the South China Sea dominated by erosion, 2004–2018. Geomorphology 344, 60–74. https://doi.org/10.1016/j.geomorph.2019.07.016
Zhang, K., Yang, F., Zhao, C., Feng, C., 2016. Using robust correlation matching to estimate sand-wave migration in Monterey Submarine Canyon, California. Mar. Geol. 376, 102–108. https://doi.org/10.1016/j.margeo.2016.04.002

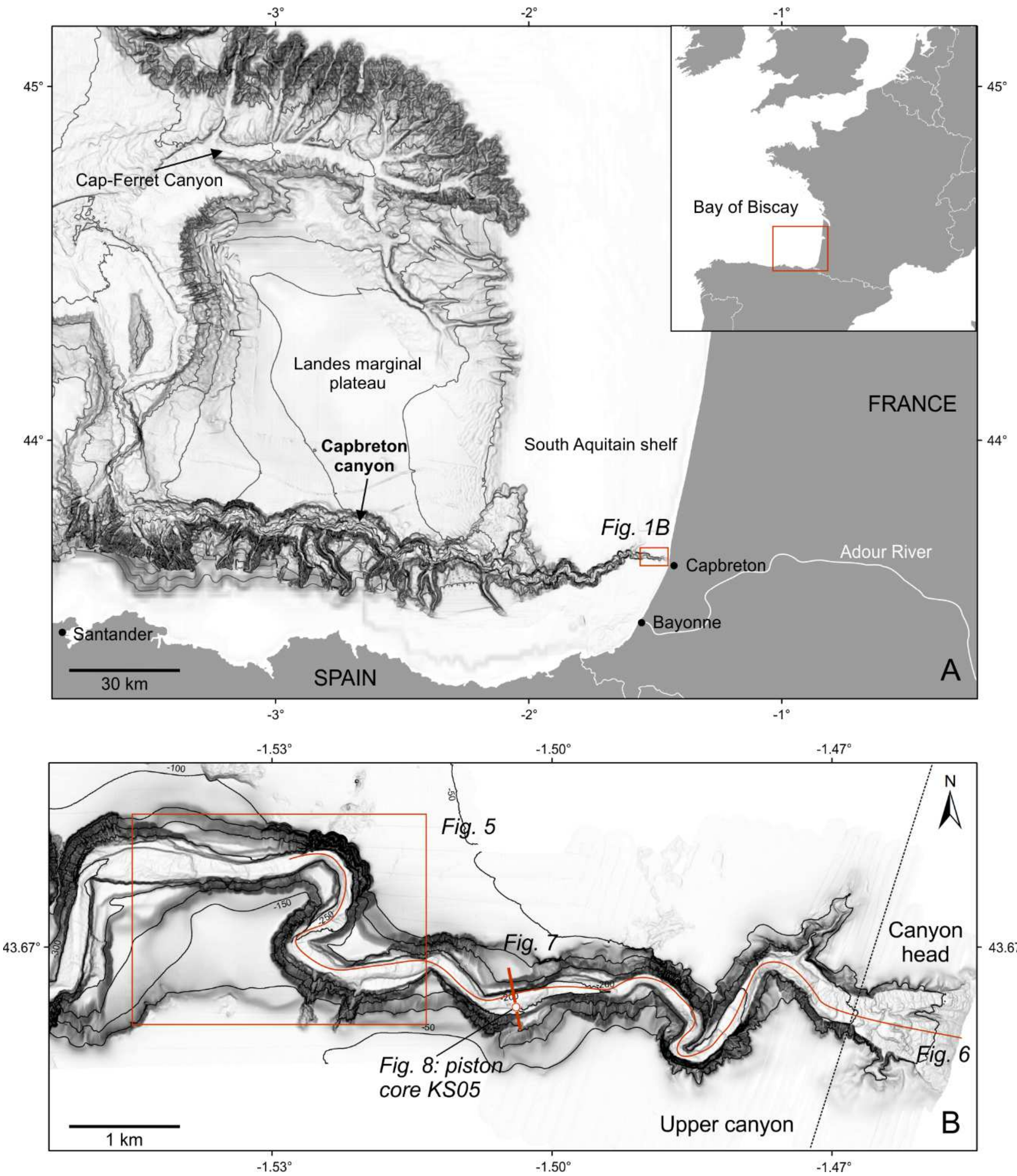

Figure 1. (A) Location of the study area in the Bay of Biscay. (B) Detailed bathymetry of the upper part of the Capbreton canyon.

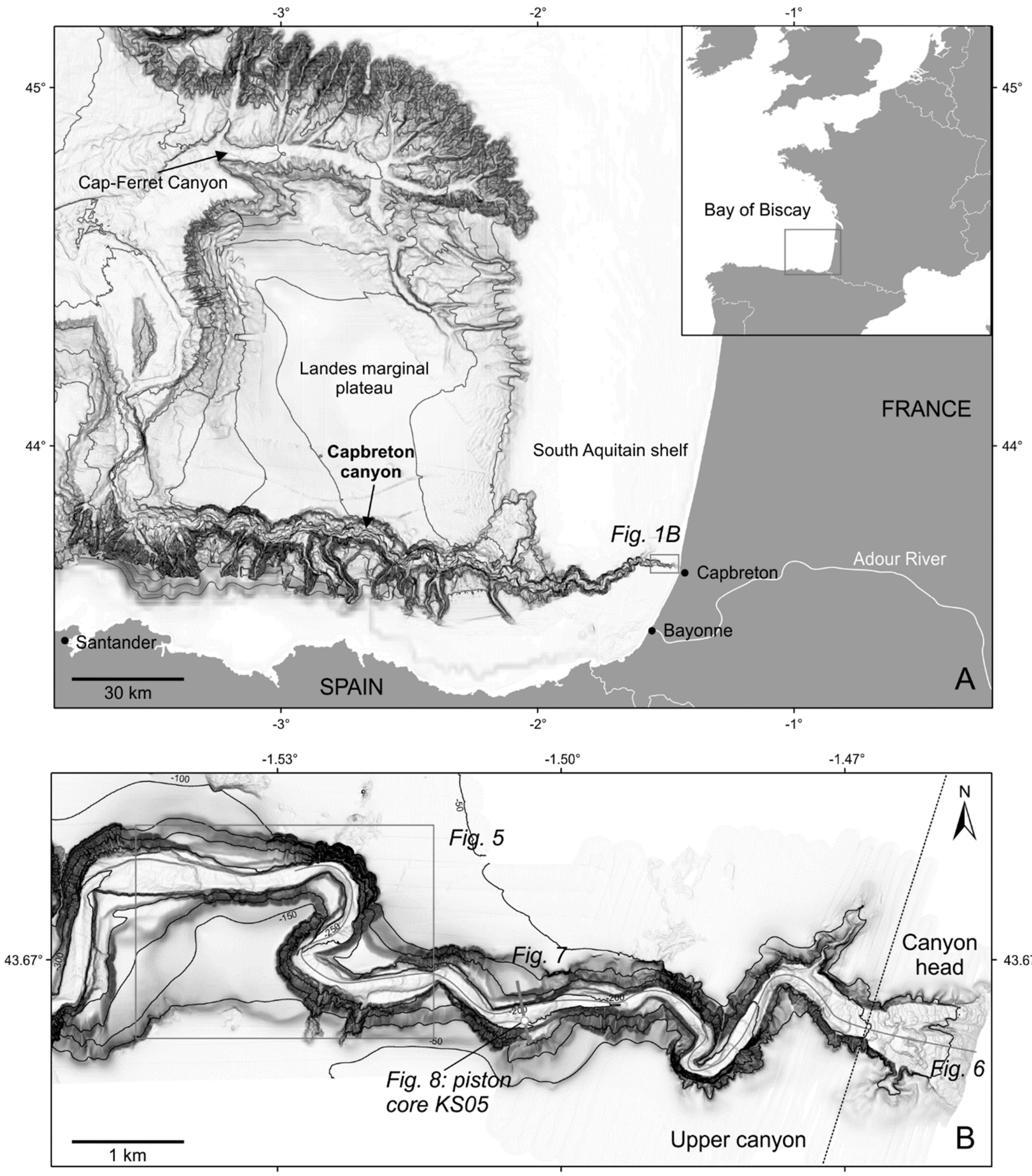

Figure 1. (A) Location of the study area in the Bay of Biscay. (B) Detailed bathymetry of the upper part of the Capbreton canyon. (A colour version of this figure is available in the web version of this paper)

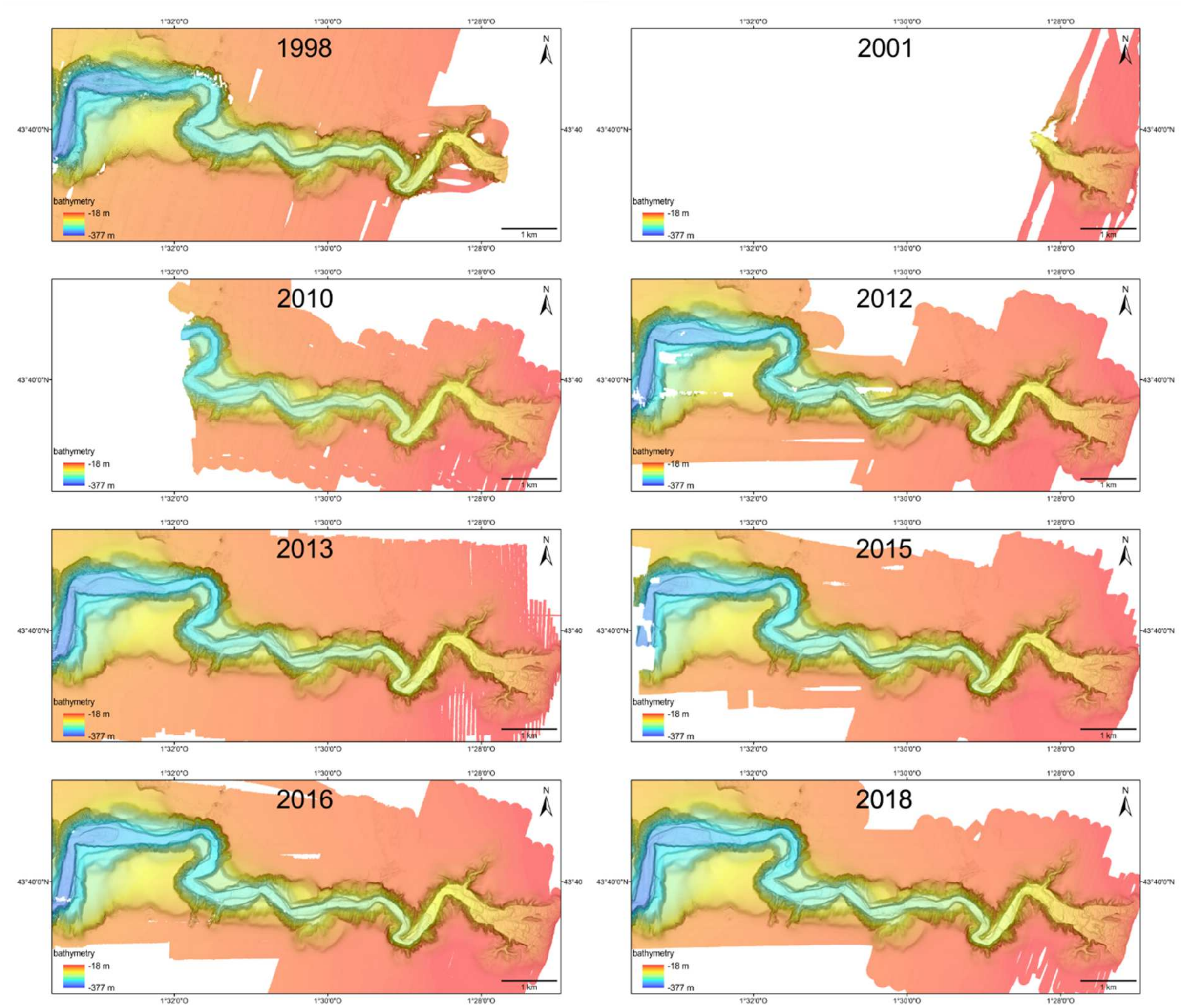

Figure 2. Bathymetric surveys of the study area acquired between 1998 and 2018.

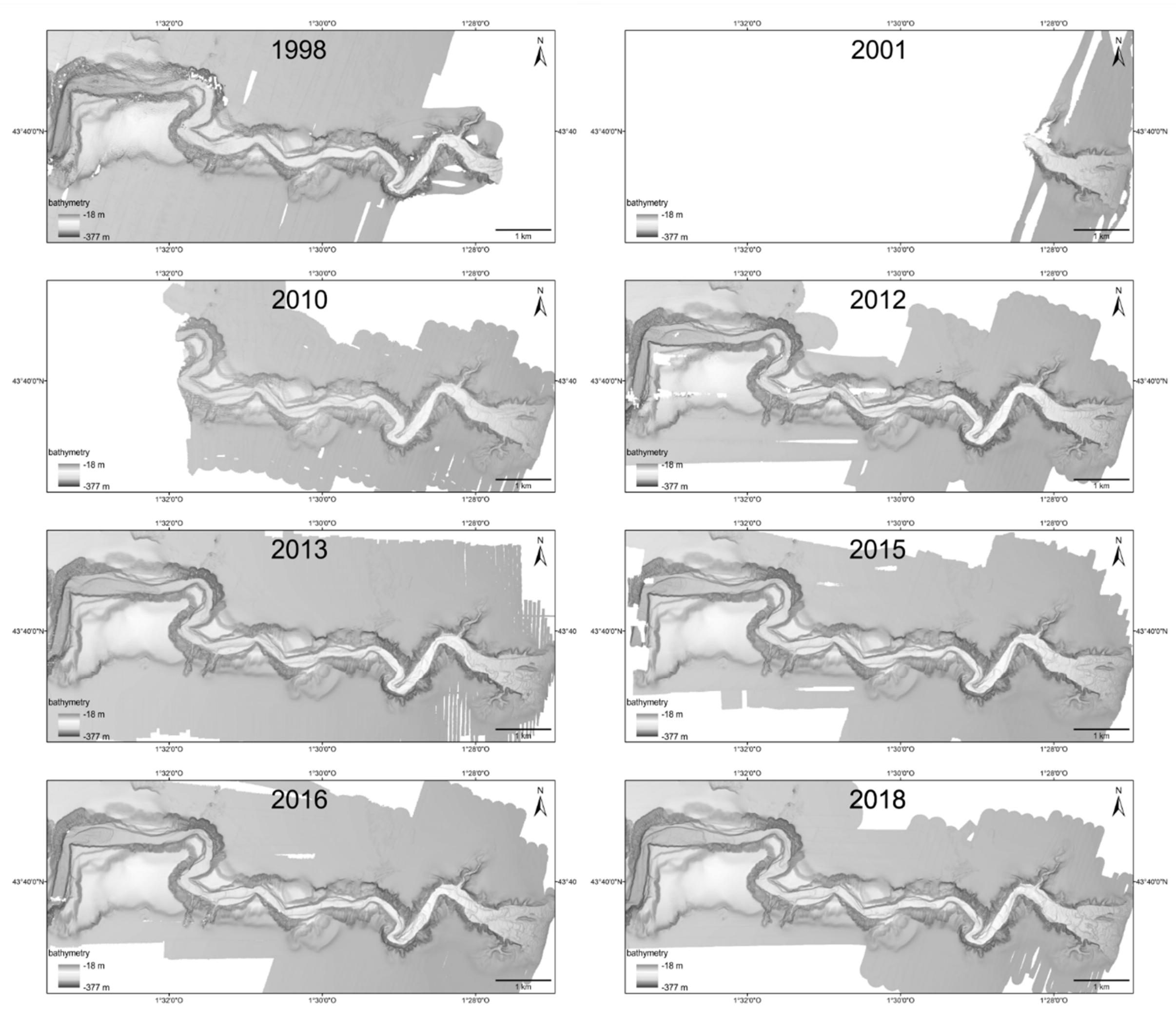

Figure 2. Bathymetric surveys of the study area acquired between 1998 and 2018. (A colour version of this figure is available in the web version of this paper)

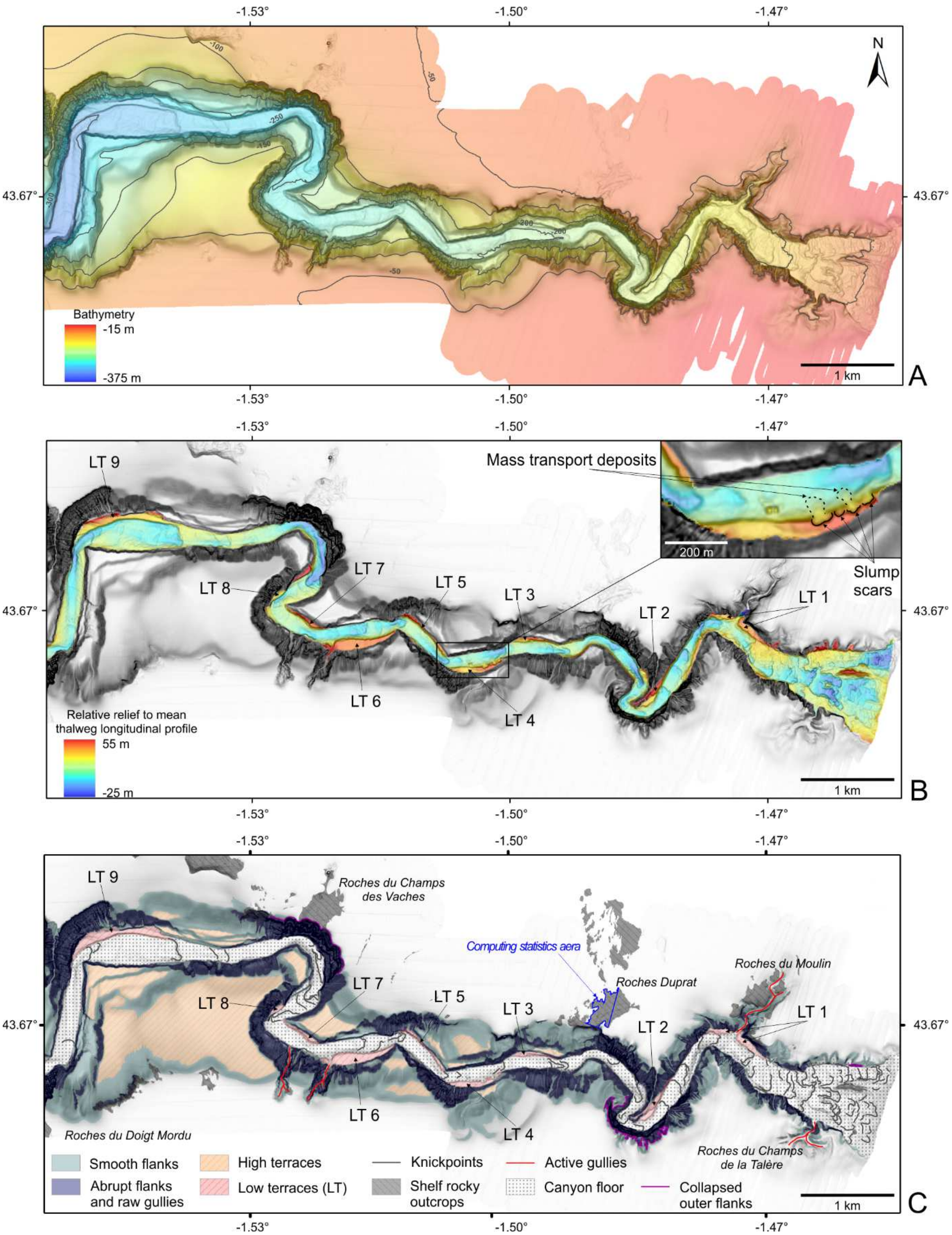

Figure 3. (A) Bathymetric survey of the study area acquired in May 2018 during the SEDYMAQ 4 cruise. (B) Relative relief to mean thalweg longitudinal profile. (C) Morphological interpretation of the Capbreton canyon upper part. Blue area corresponds to a specific area of consolidated sediments and authigenic carbonates used for statistics on repeat survey observations to validates the depth uncertainty.

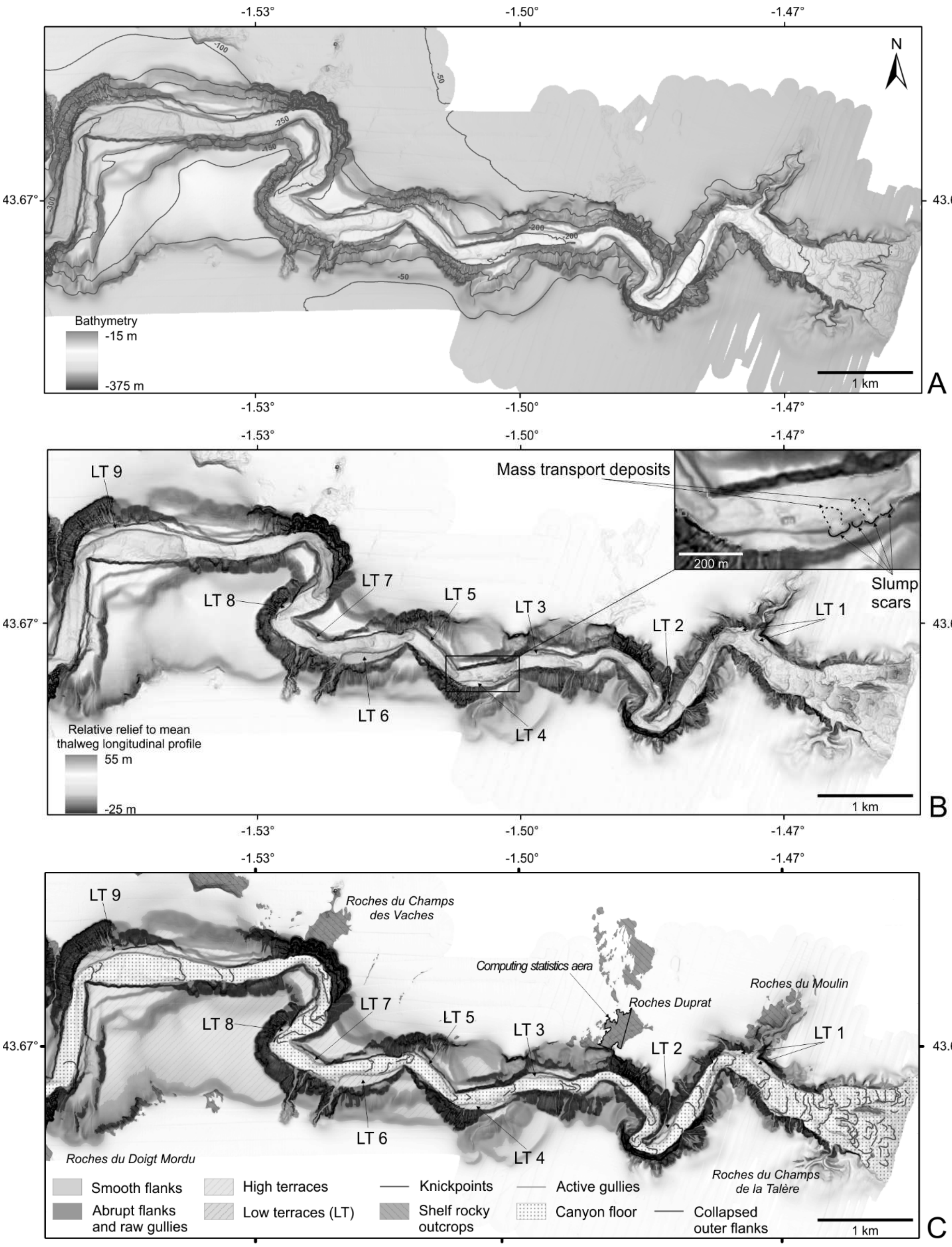

Figure 3. (A) Bathymetric survey of the study area acquired in May 2018 during the SEDYMAQ 4 cruise. (B) Relative relief to mean thalweg longitudinal profile. (C) Morphological interpretation of the Capbreton canyon upper part. Blue area corresponds to a specific area of consolidated sediments and authigenic carbonates used for statistics on repeat survey observations to validates the depth uncertainty. (A colour version of this figure is available in the web version of this paper)

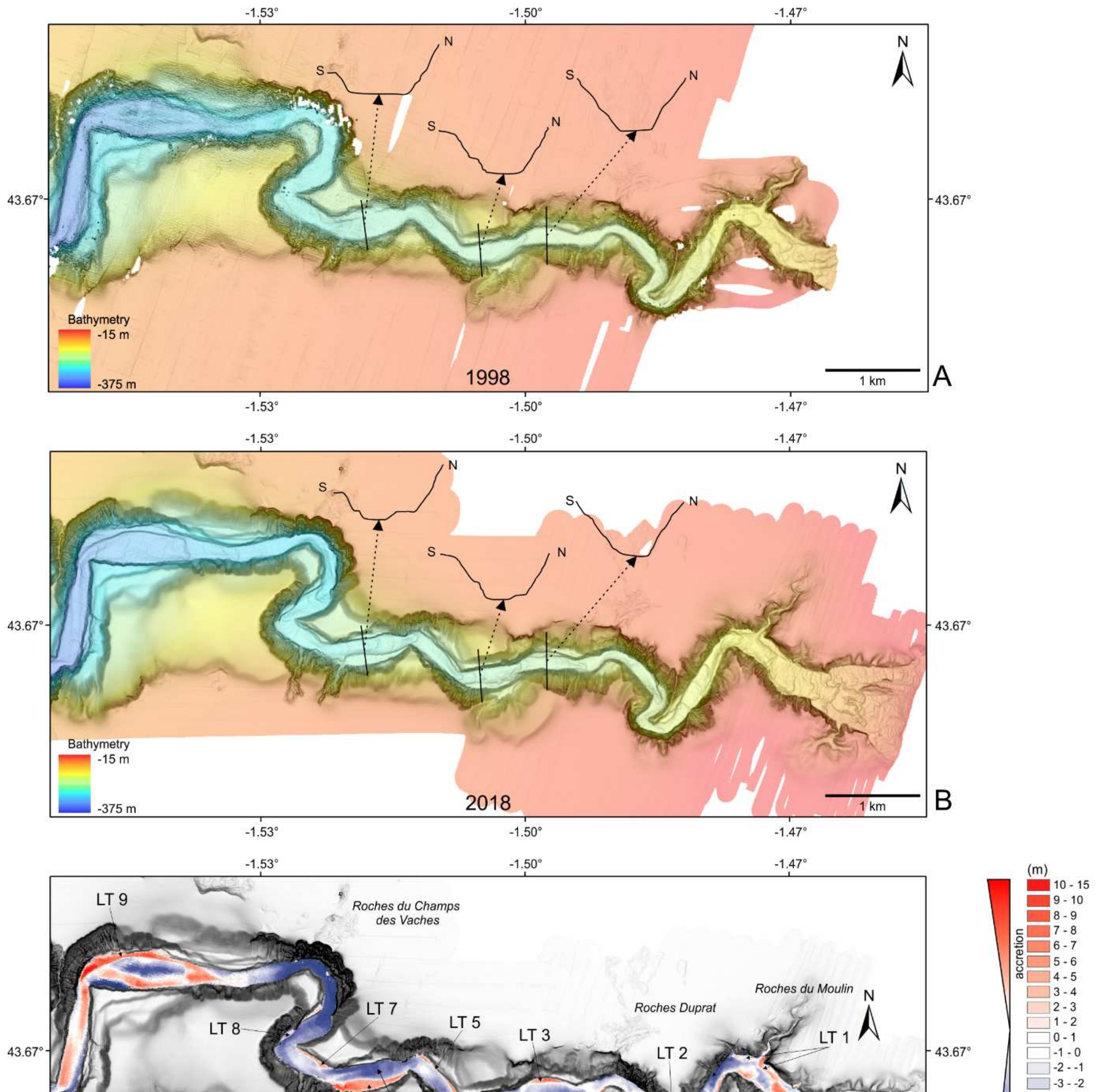

Figure 4. (A) Bathymetric survey of the study area acquired in August 1998 during the ITSAS 1 cruise including 3 cross sections. (B) Bathymetric survey of the study area acquired in May 2018 during the SEDYMAQ 4 cruise including the same 3 cross sections. (C) Bathymetric differential (May 2018 (B) minus August 1998 (A)) showing the deepening of the axial channel and the construction of recent terraces.

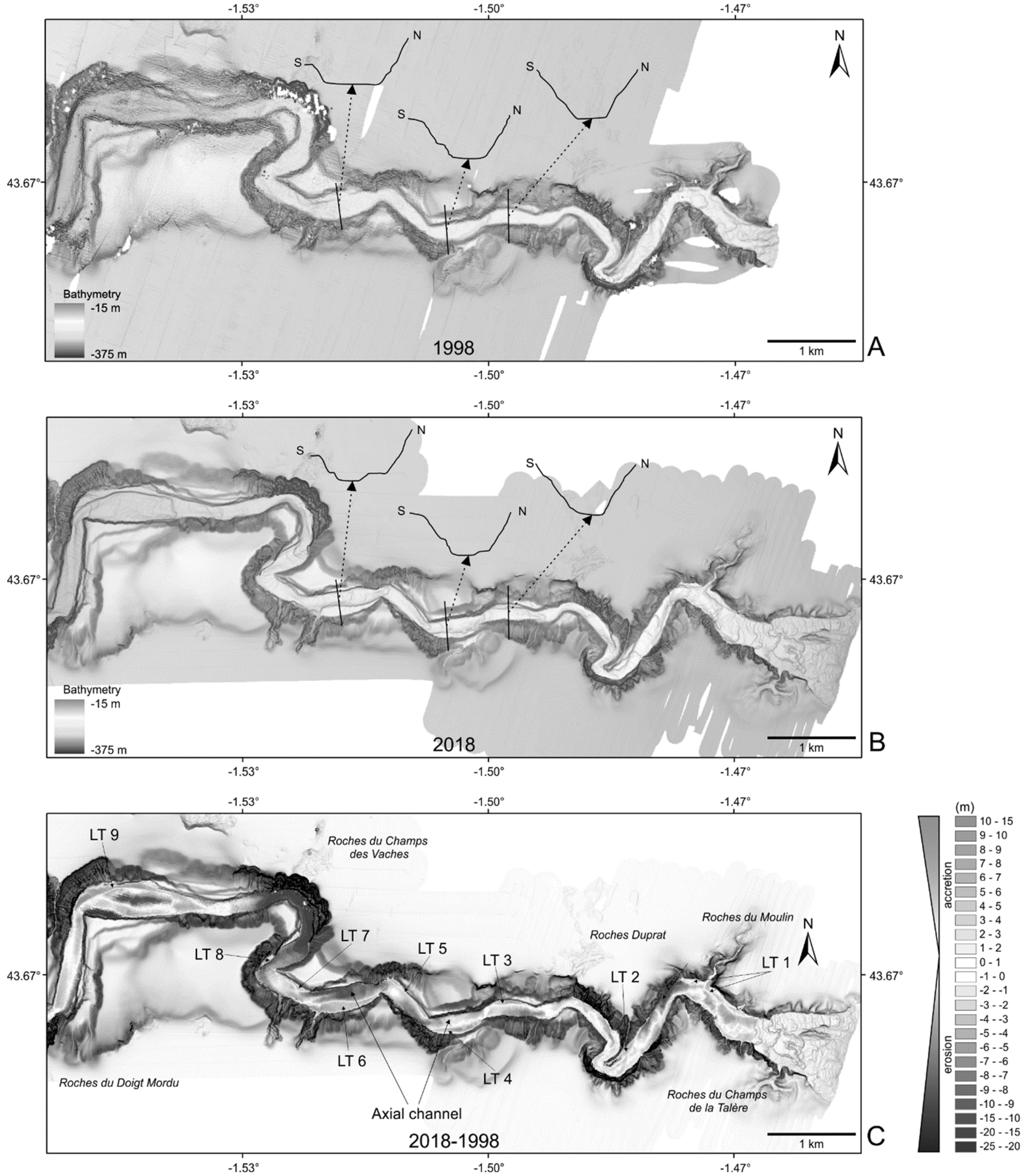

Figure 4. (A) Bathymetric survey of the study area acquired in August 1998 during the ITSAS 1 cruise including 3 cross sections. (B) Bathymetric survey of the study area acquired in May 2018 during the SEDYMAQ 4 cruise including the same 3 cross sections. (C) Bathymetric differential (May 2018 (B) minus August 1998 (A)) showing the deepening of the axial channel and the construction of recent terraces. (A colour version of this figure is available in the web version of this paper)

869

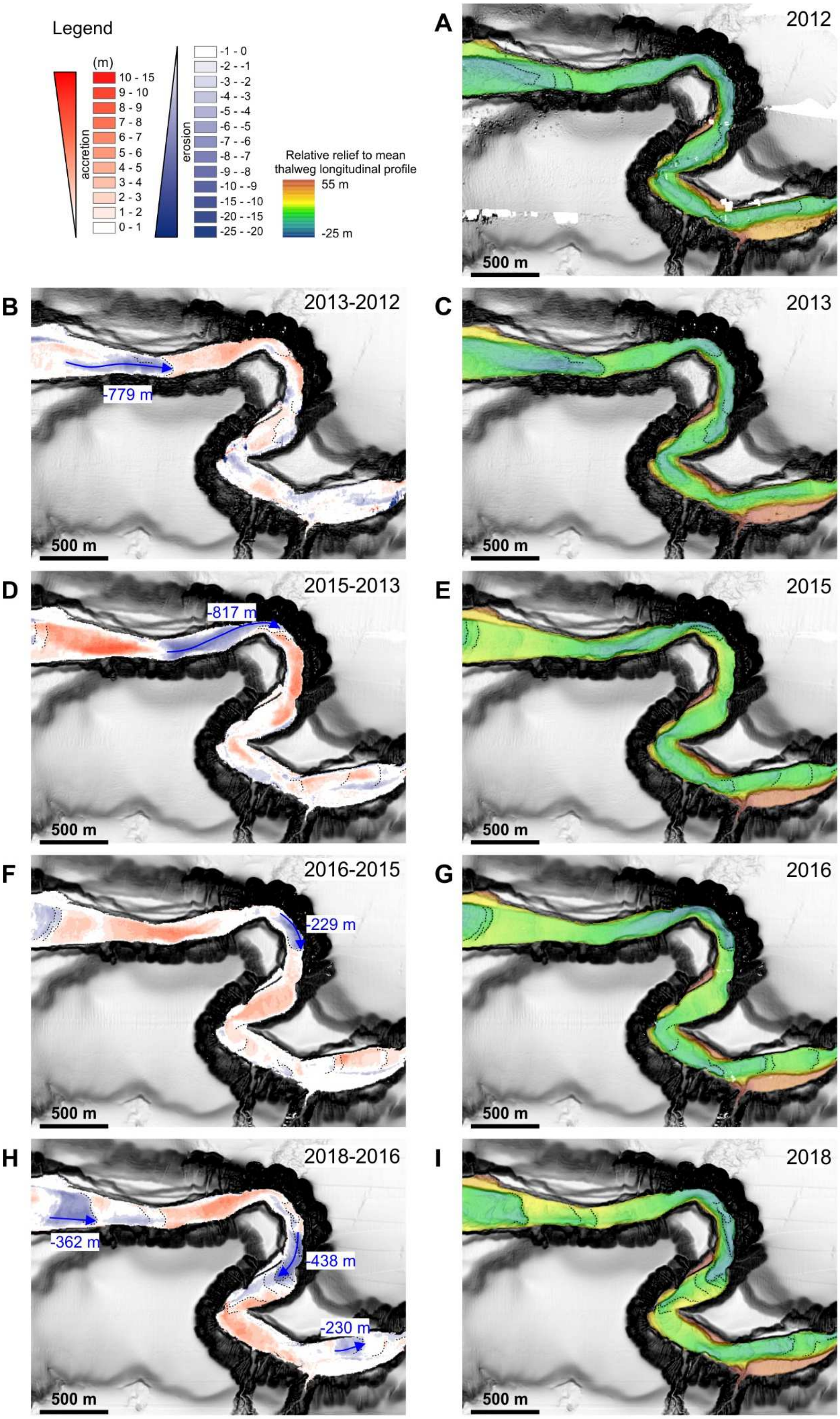

Legend
(m)
10 - 15
9 - 10
8 - 9
7 - 8
6 - 7
5 - 6
4 - 5
3 - 4
2 - 3
1 - 2
0 - 1
accretion
-1 - 0
-2 - -1
-3 - -2
-4 - -3
-5 - -4
-6 - -5
-7 - -6
-8 - -7
-9 - -8
-10 - -9
-15 - -10
-20 - -15
-25 - -20
erosion
Relative relief to mean thalweg longitudinal profile
55 m
-25 m
A
2012
500 m
B
2013-2012
-779 m
500 m
C
2013
500 m
D
2015-2013
-817 m
500 m
E
2015
500 m
F
2016-2015
-229 m
500 m
G
2016
500 m
H
2018-2016
-362 m
-438 m
-230 m
500 m
I
2018
500 m

Figure 5. Evolution of knickpoints in a distal meander of the upper part of the Capbreton canyon (see location on Figure 1). Left illustrations (B, D, F, H): representations of the bathymetric differentials between 2013/2012 (B), 2015/2013 (D), 2016/2015 (F) and 2018/2016 (H). Blue arrows represent the upstream migration of knickpoints (m). Right illustrations (A, C, E, G, I): relative relief to mean thalweg longitudinal profile in2012 (A), 2013 (C), 2015 (E), 2016 (G) and 2018 (I).

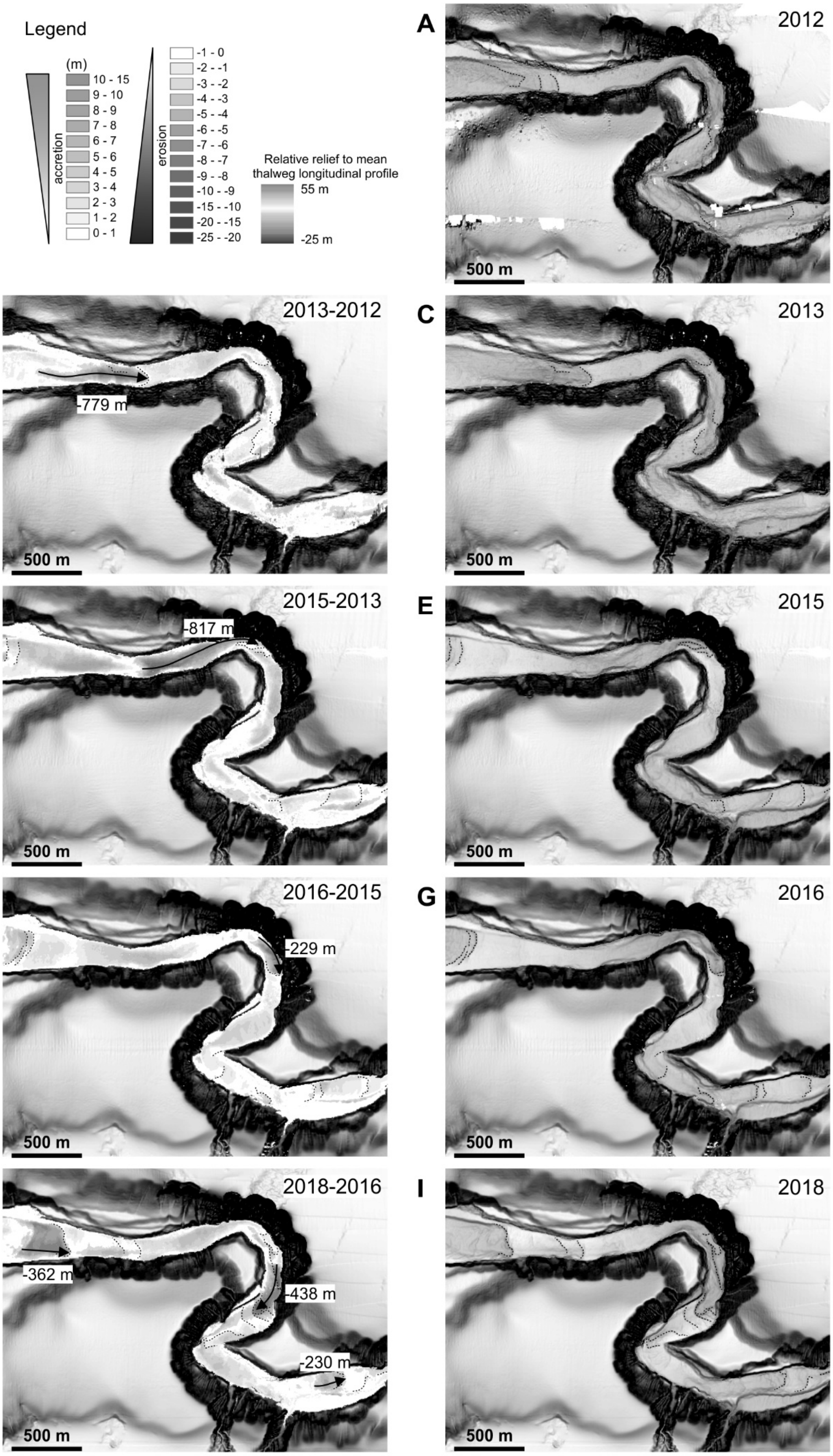

Legend
(m)
10 - 15
9 - 10
8 - 9
7 - 8
6 - 7
5 - 6
4 - 5
3 - 4
2 - 3
1 - 2
0 - 1
accretion
-1 - 0
-2 - -1
-3 - -2
-4 - -3
-5 - -4
-6 - -5
-7 - -6
-8 - -7
-9 - -8
-10 - -9
-15 - -10
-20 - -15
-25 - -20
erosion
Relative relief to mean thalweg longitudinal profile
55 m
-25 m
A
2012
500 m
B
2013-2012
-779 m
500 m
C
2013
500 m
D
2015-2013
-817 m
500 m
E
2015
500 m
F
2016-2015
-229 m
500 m
G
2016
500 m
H
2018-2016
-362 m
-438 m
-230 m
500 m
I
2018
500 m

876

Figure 5. Evolution of knickpoints in a distal meander of the upper part of the Capbreton canyon (see location on Figure 1). Left illustrations (B, D, F, H): representations of the bathymetric differentials between 2013/2012 (B), 2015/2013 (D), 2016/2015 (F) and 2018/2016 (H). Blue arrows represent the upstream migration of knickpoints (m). Right illustrations (A, C, E, G, I): relative relief to mean thalweg longitudinal profile in2012 (A), 2013 (C), 2015 (E), 2016 (G) and 2018 (I). (A colour version of this figure is available in the web version of this paper)

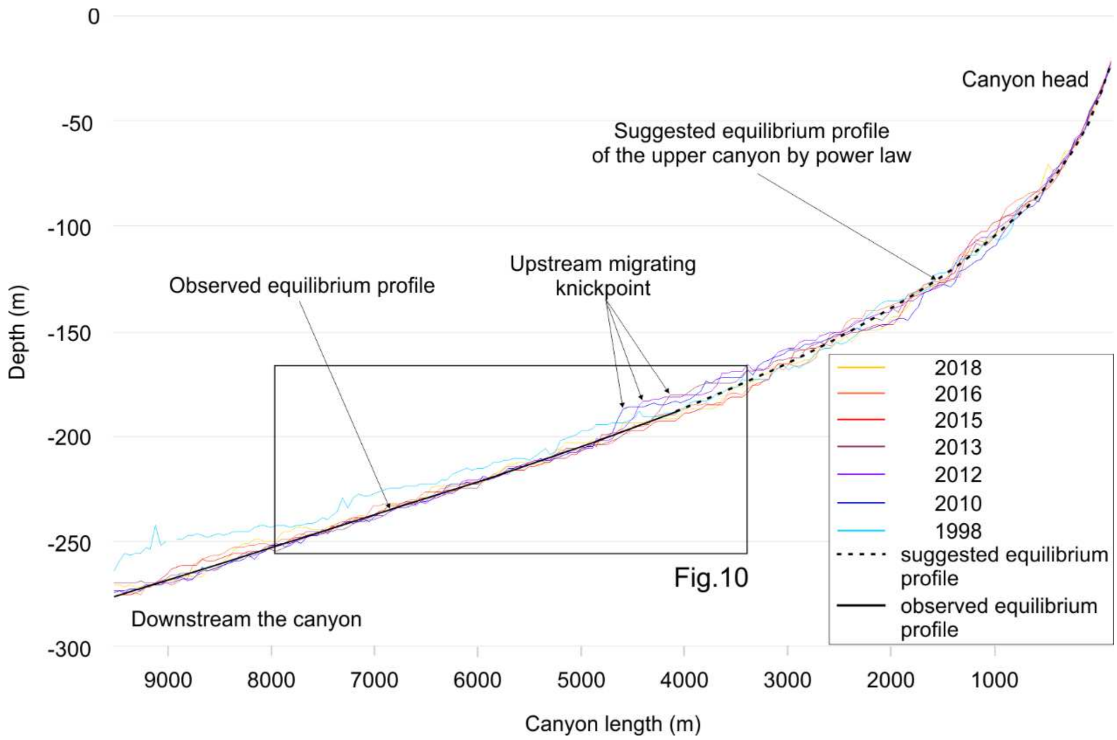

Figure 6. Evolution of the mean thalweg longitudinal profile from 1998 to 2018 (see location on Figure 1). The equilibrium profile was established after observation by a simple mean of longitudinal profiles extracted from DEMs between 2010 to 2018 and from 4 to 9.5 km downstream the head. Upstream, the equilibrium profile is proposed from a simple depth(z)-distance(d) relation power law corresponding to $z \approx -4.82d^{1.55}$.

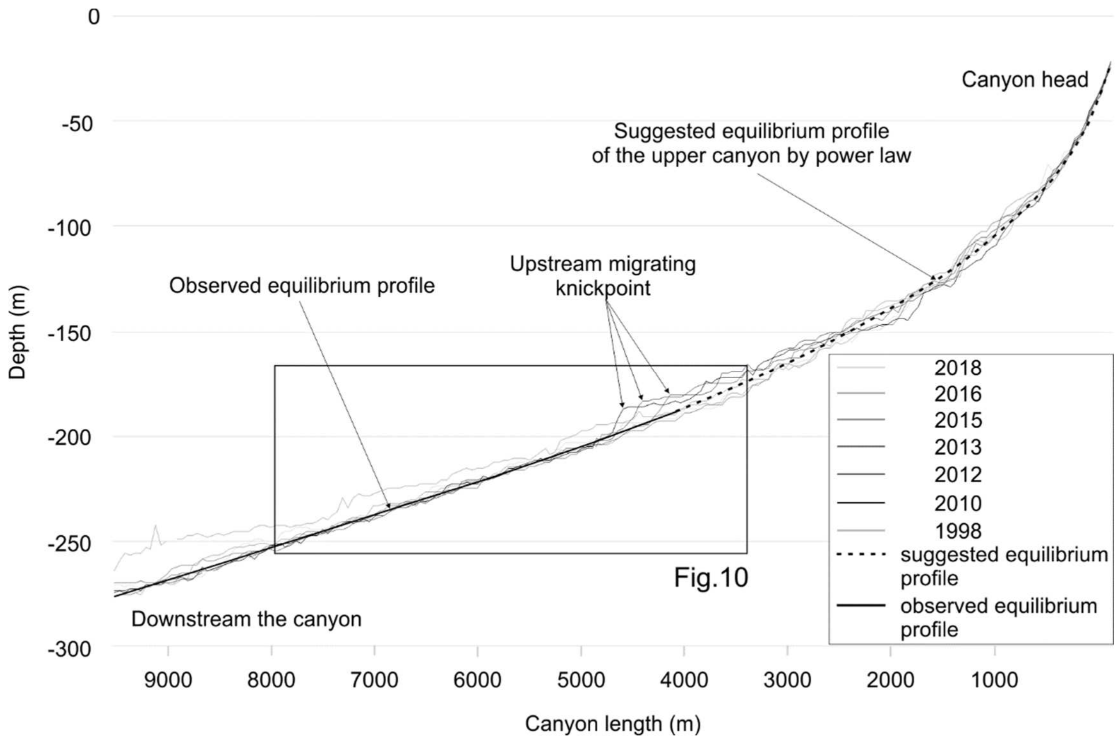

Figure 6. Evolution of the mean thalweg longitudinal profile from 1998 to 2018 (see location on Figure 1). The equilibrium profile was established after observation by a simple mean of longitudinal profiles extracted from DEMs between 2010 to 2018 and from 4 to 9.5 km downstream the head. Upstream, the equilibrium profile is proposed from a simple depth(z)-distance(d) relation power law corresponding to $z \approx -4.82d^{1.55}$. (A colour version of this figure is available in the web version of this paper)

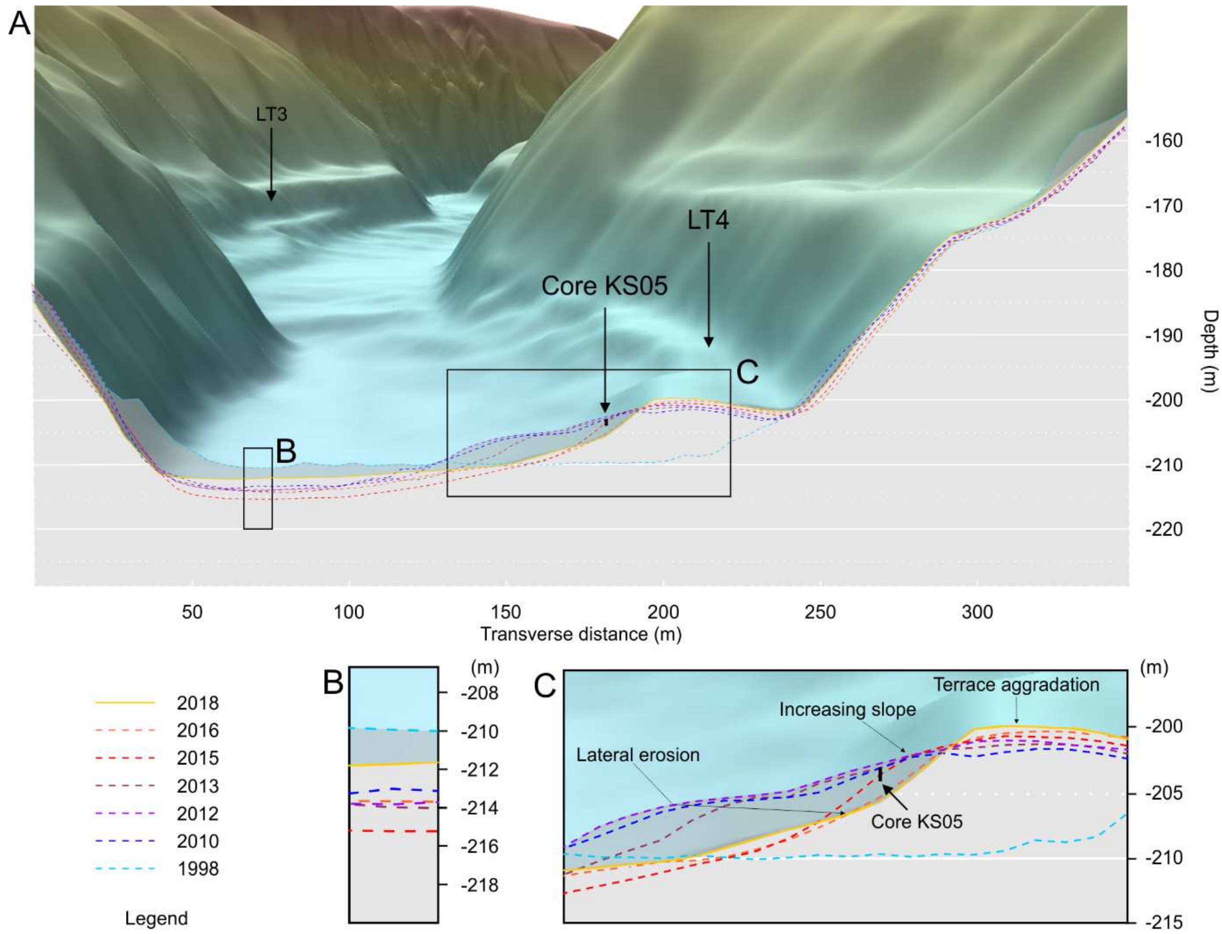

Figure 7. Thalweg evolution and construction of low terrace 4 (LT4) in the upper part of the Capbreton canyon from 1998 to 2018 (see location of the cross-section on Figure 1).

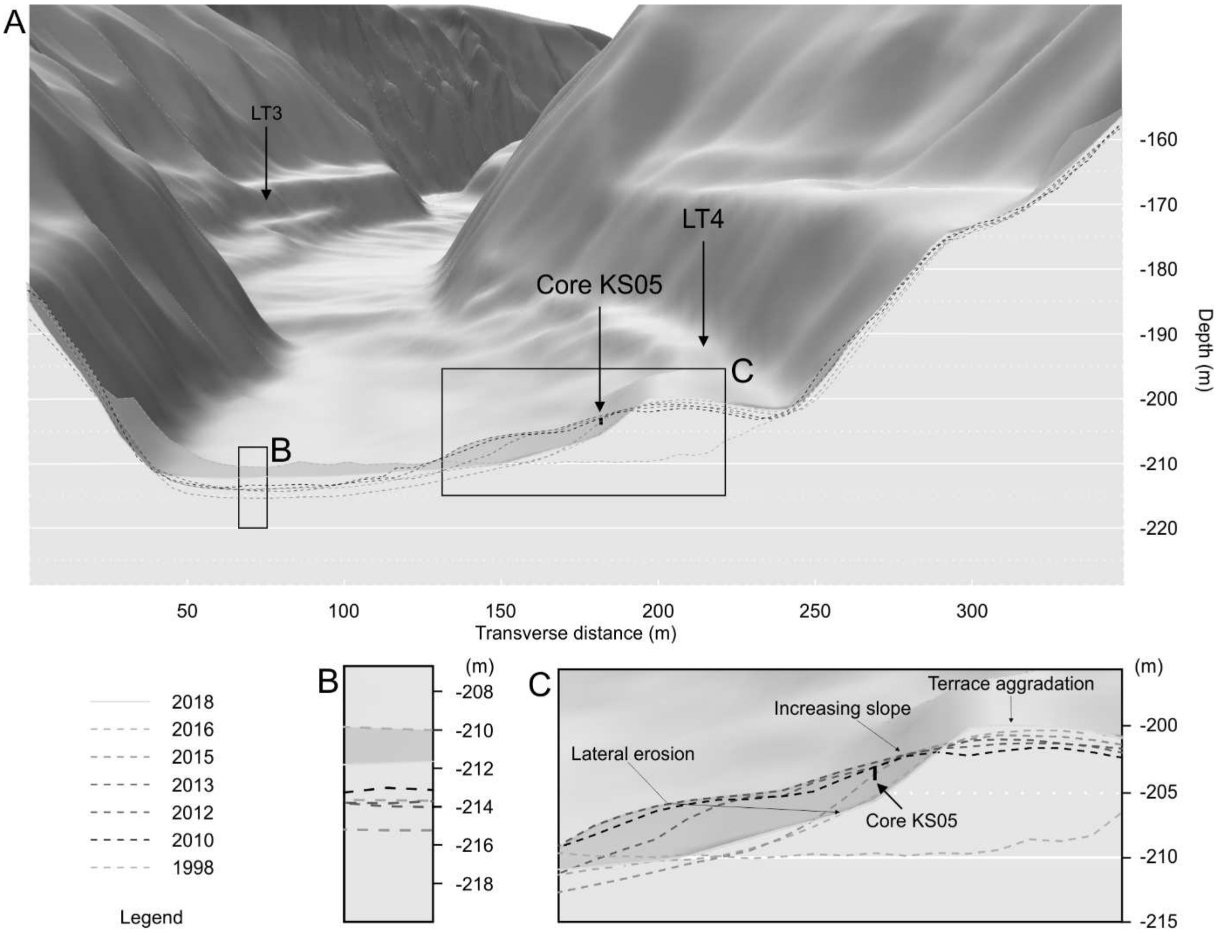

Figure 7. Thalweg evolution and construction of low terrace 4 (LT4) in the upper part of the Capbreton canyon from 1998 to 2018 (see location of the cross-section on Figure 1). (A colour version of this figure is available in the web version of this paper)

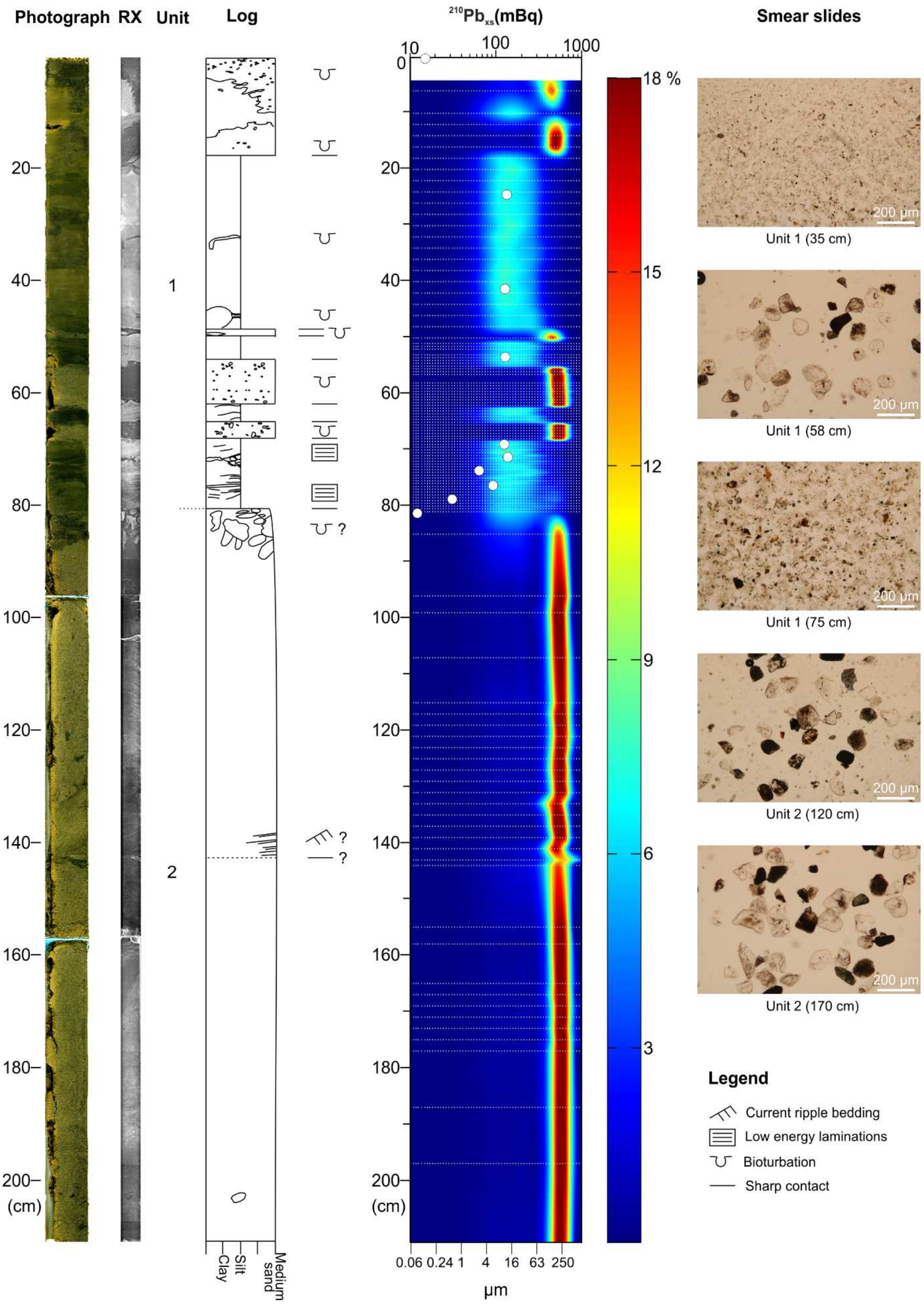

Figure 8. From left to right: photography, RX imagery, interpreted synthetic log, granulometry and smear slides of core KS05 (see location on figure 1 and figure 7). White dots on granulometry map correspond to $^{210}Pb_{xs}$.

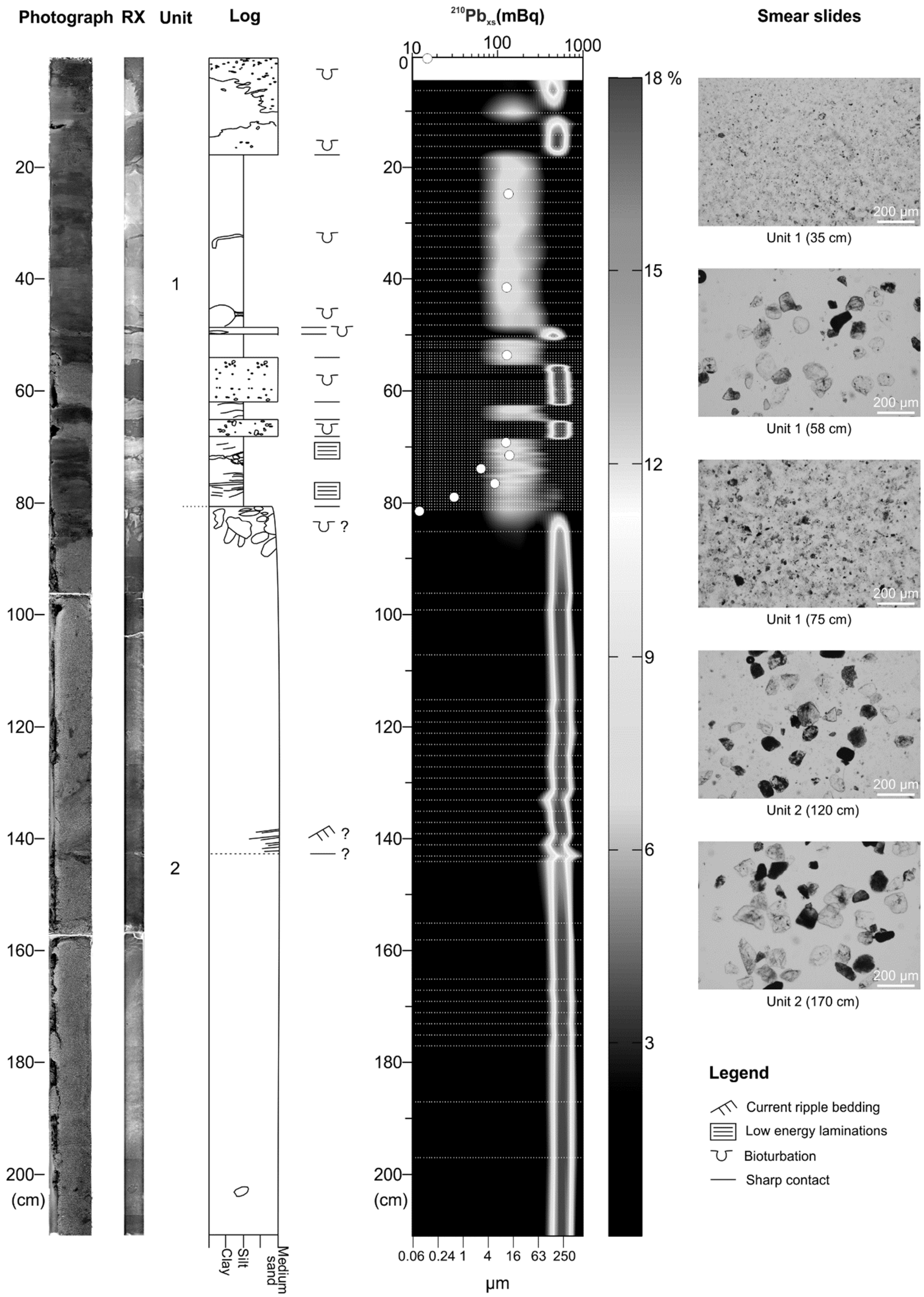

Figure 8. From left to right: photography, RX imagery, interpreted synthetic log, granulometry and smear slides of core KS05 (see location on figure 1 and figure 7). White dots on granulometry map correspond to $^{210}Pb_{xs}$. (A colour version of this figure is available in the web version of this paper)

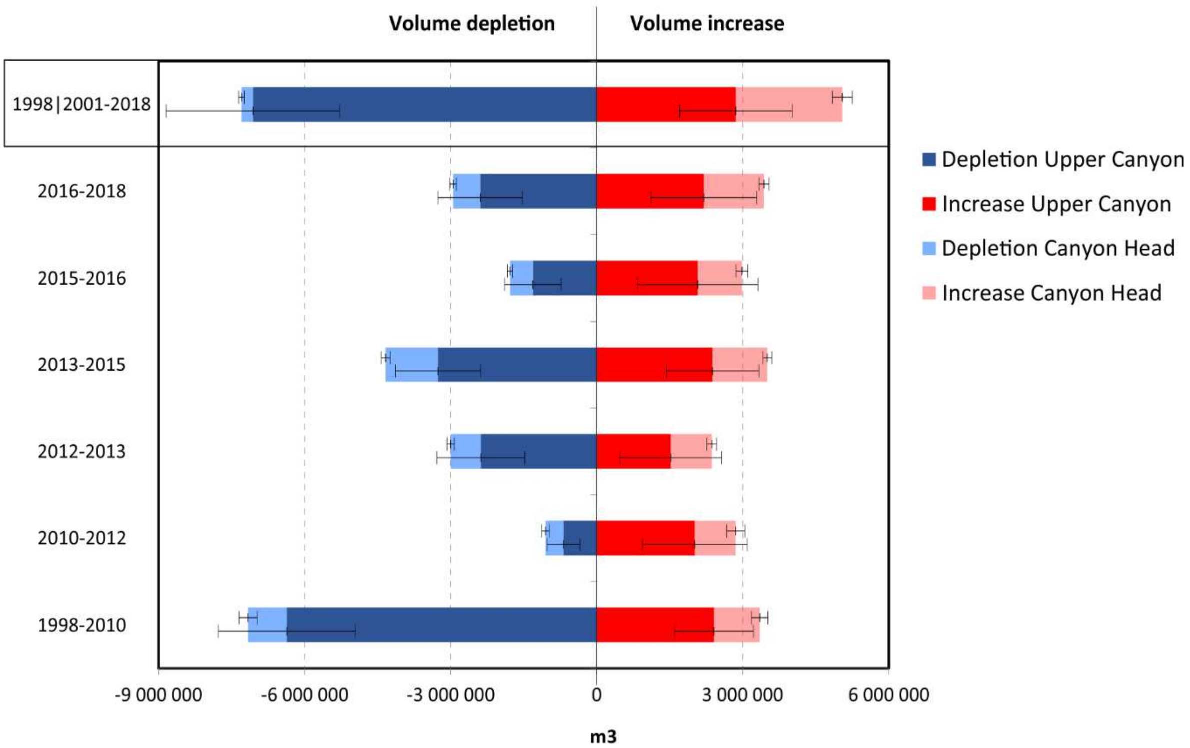

Figure 9. Representation of sediment volumes (including error bars) which transit through the upper Capbreton Canyon and its head over 20 years (from 1998 to 2018).

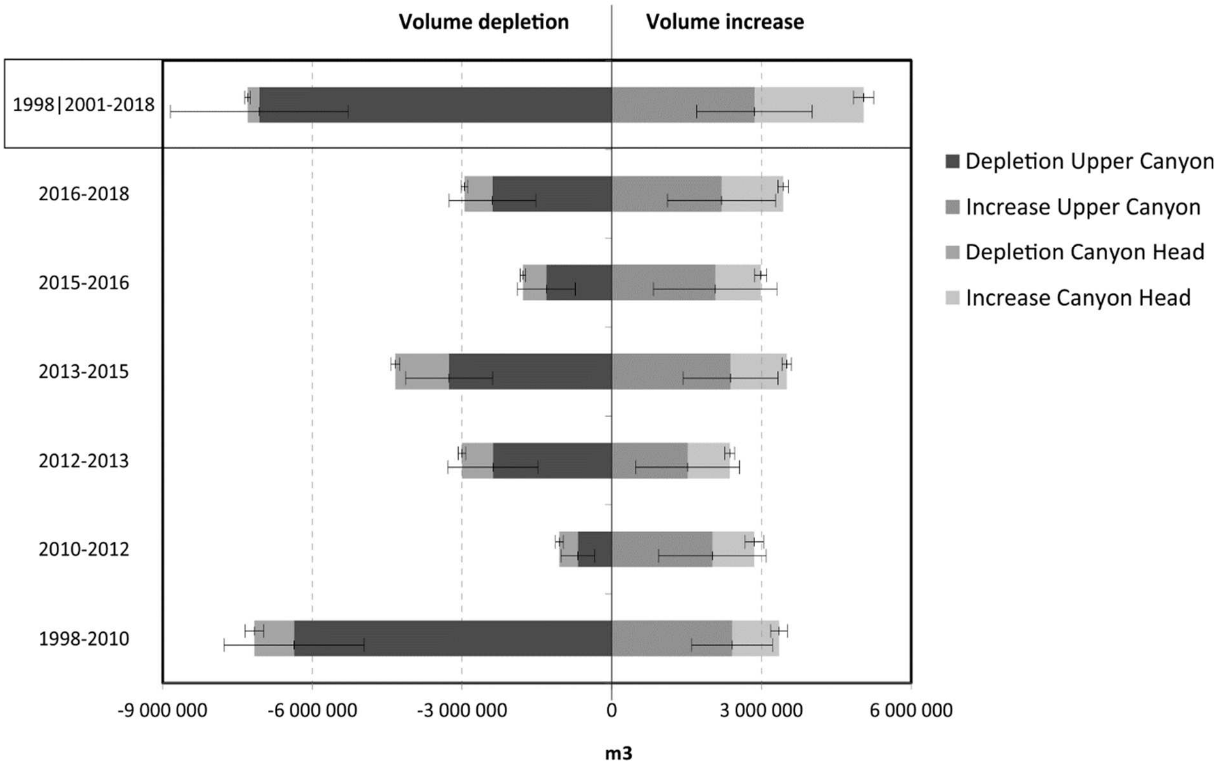

Figure 9. Representation of sediment volumes (including error bars) which transit through the upper Capbreton Canyon and its head over 20 years (from 1998 to 2018). (A colour version of this figure is available in the web version of this paper)

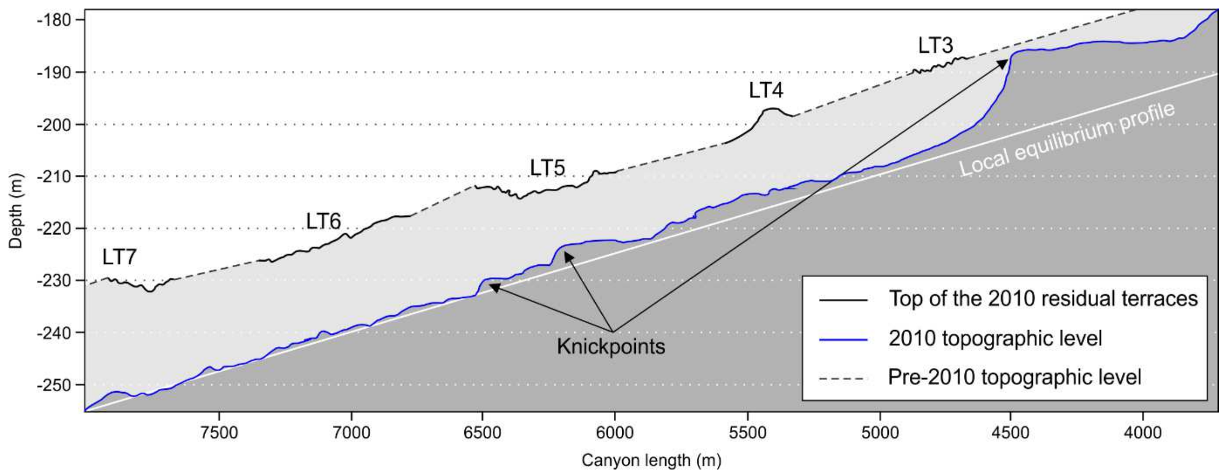

Figure 10. 2010 longitudinal profiles of the thalweg and low terraces 3, 4, 5, 6 and 7 (see location on Figure 6) suggesting the homogenous deposition of sediment in the Capbreton before 2010, and followed by its reshaping by the retrogressive erosion and upstream migration of knickpoints.

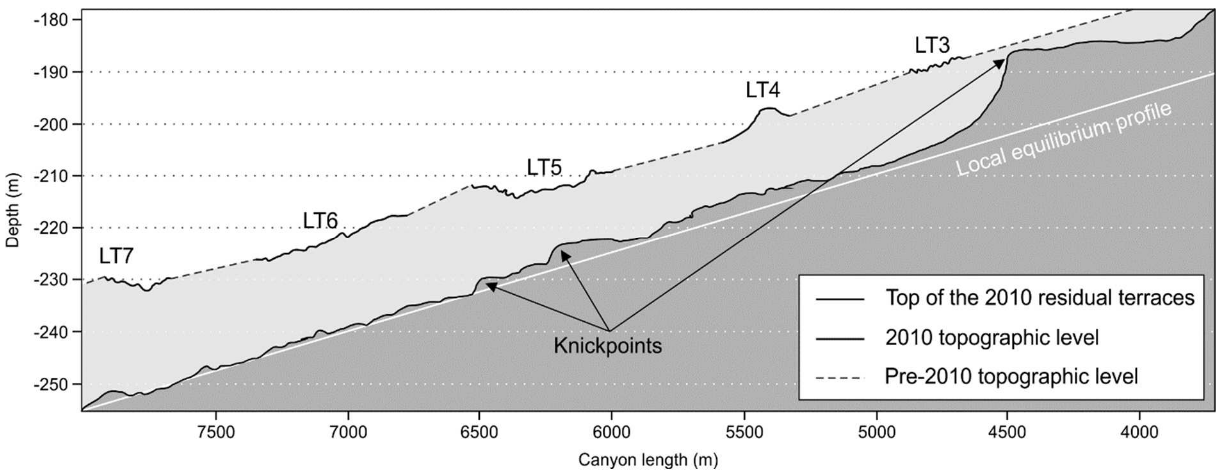

Figure 10. 2010 longitudinal profiles of the thalweg and low terraces 3, 4, 5, 6 and 7 (see location on Figure 6) suggesting the homogenous deposition of sediment in the Capbreton before 2010, and followed by its reshaping by the retrogressive erosion and upstream migration of knickpoints. (A colour version of this figure is available in the web version of this paper)

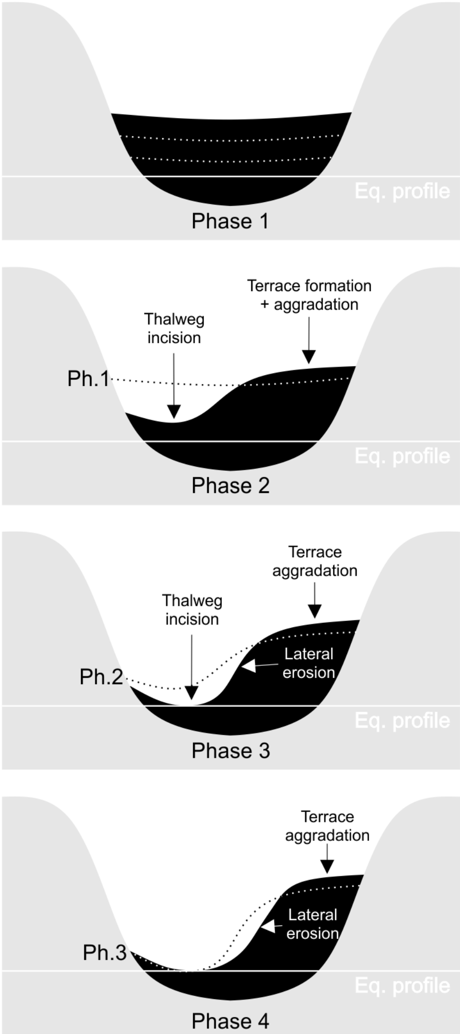

Figure 11. Conceptual model describing the formation of the low terrace.

942

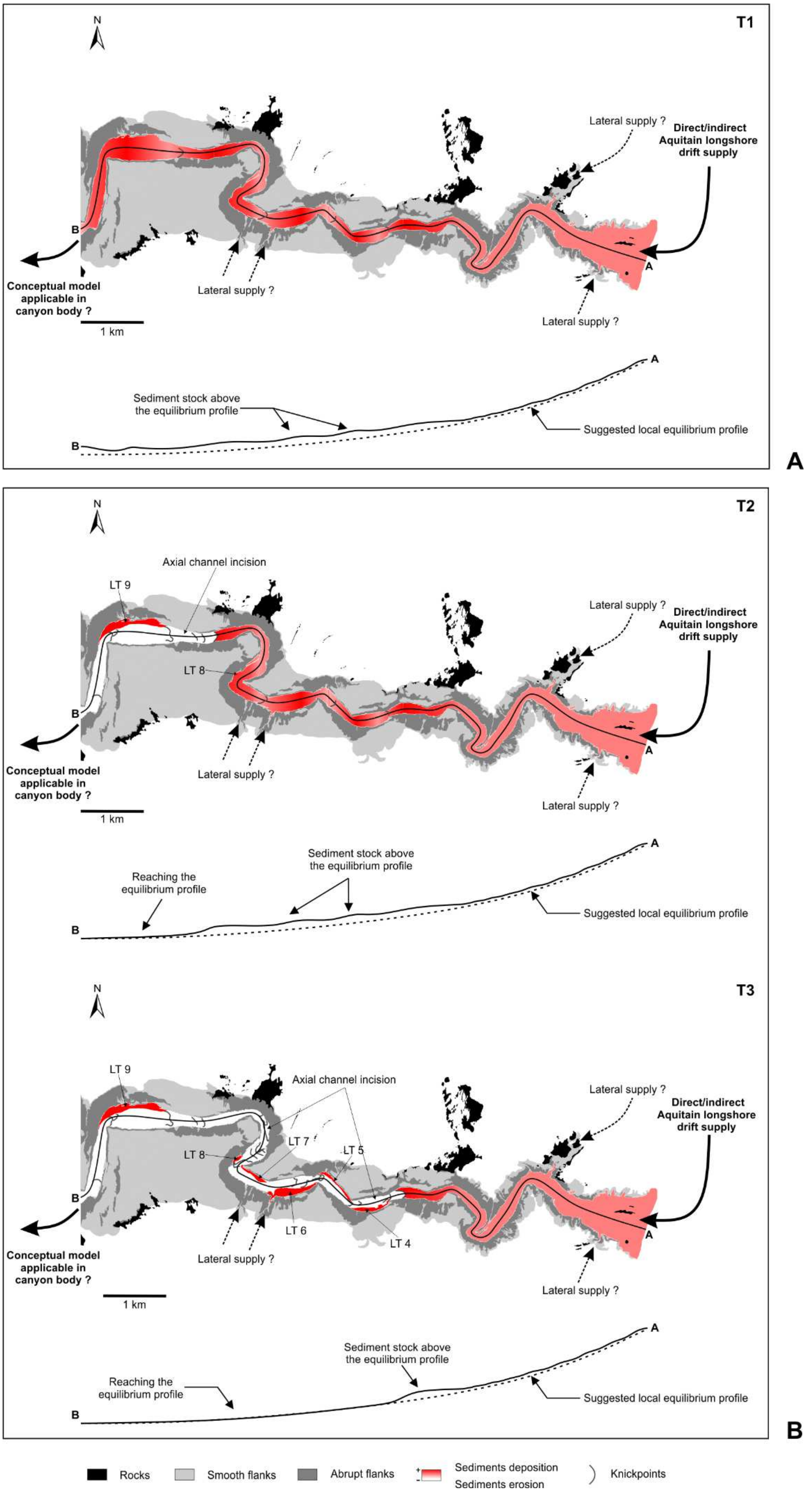

T1
N
Lateral supply ?
Direct/indirect Aquitain longshore drift supply
B
A
Conceptual model applicable in canyon body ?
Lateral supply ?
Lateral supply ?
1 km
Sediment stock above the equilibrium profile
Suggested local equilibrium profile
A
T2
Axial channel incision
LT 9
LT 8
Reaching the equilibrium profile
T3
LT 7
LT 5
LT 6
LT 4
B
Rocks
Smooth flanks
Abrupt flanks
Sediments deposition
Sediments erosion
Knickpoints

Figure 12: Representation of the two distinct modes which can be observed in the very upper part: (A) times of flat thalweg where the sedimentary stock is above the local equilibrium profile and (B) times of channel incision associated to lateral low terraces construction where the canyon is reaching its a transient and local equilibrium profile through the upstream migration of knickpoints.

948

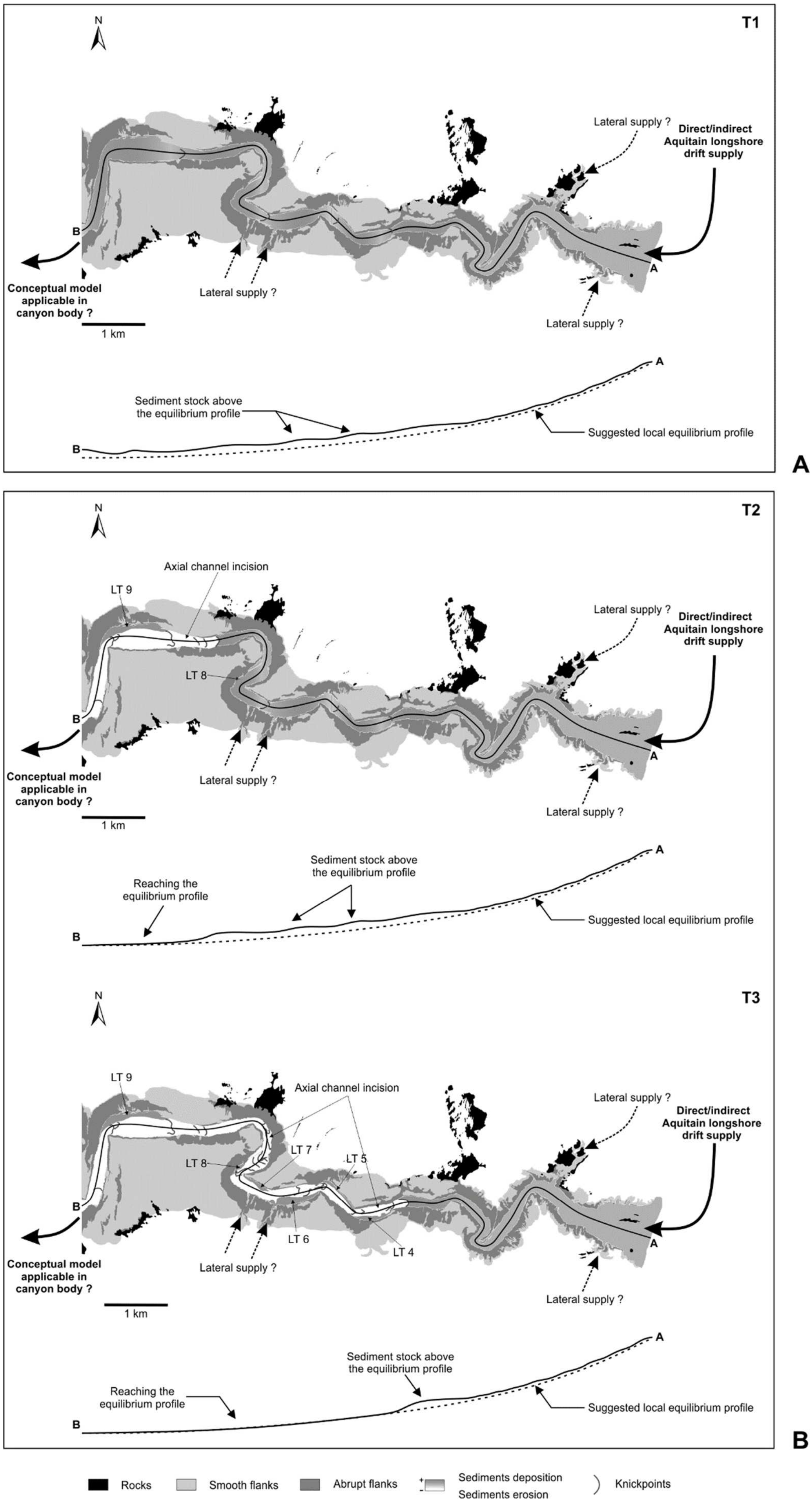
T1
Lateral supply ?
Direct/indirect Aquitain longshore drift supply
B
A
Conceptual model applicable in canyon body ?
Lateral supply ?
Lateral supply ?
1 km
Sediment stock above the equilibrium profile
Suggested local equilibrium profile
A
T2
Axial channel incision
LT 9
LT 8
Lateral supply ?
Direct/indirect Aquitain longshore drift supply
Conceptual model applicable in canyon body ?
Lateral supply ?
Lateral supply ?
1 km
Sediment stock above the equilibrium profile
Reaching the equilibrium profile
Suggested local equilibrium profile
T3
LT 9
Axial channel incision
LT 8
LT 7
LT 5
LT 6
LT 4
Lateral supply ?
Direct/indirect Aquitain longshore drift supply
Conceptual model applicable in canyon body ?
Lateral supply ?
Lateral supply ?
1 km
Sediment stock above the equilibrium profile
Reaching the equilibrium profile
Suggested local equilibrium profile
B
Rocks
Smooth flanks
Abrupt flanks
Sediments deposition
Sediments erosion
Knickpoints

Figure 12: Representation of the two distinct modes which can be observed in the very upper part: (A) times of flat thalweg where the sedimentary stock is above the local equilibrium profile and (B) times of channel incision associated to lateral low terraces construction where the canyon is reaching its a transient and local equilibrium profile through the upstream migration of knickpoints. (A colour version of this figure is available in the web version of this paper)

Year	Month	Name	Multibeam echo sounder
1998	August	Itsas 1	EM1000
2001	May	Itsas V	EM1000
2010	May	Sedymaq 2	EM1000
2012	June	Sedymaq 3	EM2040
2013	September	Protevs-Dunes	EM1002/EM2040
2015	August	Volt2015	EM2040
2016	March	volt2016	EM2040
2018	May	Sedymaq 4	EM2040

Table 1: List of oceanic surveys conducted in the study area between 1998 and 2018.

	LT4 aggradation (m)	LT4 aggradation (m.year^{-1})	LT4 lateral erosion (m.year^{-1})	Knickpoints average upstream migration (m.year^{-1})
2012-2010	0.61 +/-1	0.29	-2.70	91
2013-2012	-0.03 +/-0.40	-0.03	-16.25	320
2015-2013	0.78 +/-0.40	0.40	-13.76	606
2016-2015	0.22 +/-0.40	0.36	-12.59	538
2018-2016	0.70 +/-0.40	0.32	-1.32	110

Table 2. Quantification and follow-up of main morphologic changes between 2010 and 2018

CANYON BODY

	Eroded **V**olume (m^3)	**EV** Surface (m^2)	m/year	+/-	**D**eposited **V**olume	**DV** Surface (m^2)	m/year	+/-	**DV**-**EV** (m^3)	m3/year	m/year	+/-	Sediment budget
2010-1998	-6369985	877200	-0.62	0.14	2410484	565450	0.36	0.12	-3959501	-337274	-0.23	0.13	Erosion
2012-2010	-679927	474825	-0.69	0.40	2013357	968300	1.00	0.53	1333430	638717	0.44	0.49	Deposition
2013-2012	-2383623	1036800	-1.83	0.69	1518841	1113325	1.08	0.74	-864782	-687681	-0.32	0.72	Erosion
2015-2013	-3262850	1027650	-1.64	0.44	2378487	1024575	1.20	0.48	-884363	-455922	-0.22	0.46	Erosion
2016-2015	-1311999	680850	-3.18	1.42	2075837	1367900	2.51	1.50	763838	1261542	0.62	1.47	Deposition
2018-2016	-2391024	949500	-1.16	0.42	2200662	1205775	0.84	0.42	-190362	-87952	-0.04	0.42	Erosion
2018-1998	-7061562	1309000	-0.32	0.08	2861281	859900	0.20	0.08	-4200280	-246242	-0.11	0.08	Erosion

CANYON HEAD

	Eroded **V**olume (m^3)	**EV** Surface (m^2)	m/year	+/-	**D**eposited **V**olume (m^3)	**DV** Surface (m^2)	m/year	+/-	**DV**-**EV** (m^3)	m3/year	m/year	+/-	Sediment budget
2010-2001	-792958	364825	-0.24	0.06	938400	368375	0.28	0.05	145442	16155	0.02	0.05	Deposition
2012-2010	-368560	242450	-0.73	0.16	844447	493475	0.82	0.18	475887	227951	0.31	0.17	Deposition
2013-2012	-615659	360350	-1.36	0.17	847577	388875	1.73	0.21	231918	184423	0.25	0.19	Deposition
2015-2013	-1072400	360850	-1.53	0.13	1124724	433475	1.34	0.11	52324	26975	0.03	0.12	Deposition
2016-2015	-471293	251775	-3.09	0.37	908753	526300	2.85	0.38	437460	722502	0.93	0.38	Deposition
2018-2016	-558364	281350	-0.92	0.11	1235107	452275	1.26	0.11	676744	312673	0.43	0.11	Deposition
2018-2001	-236731	163425	-0.08	0.02	2182478	564075	0.23	0.02	1945747	114070	0.16	0.02	Deposition

Table 3. Accurate volume quantification of sediment deposition and erosion in the upper canyon and head canyon floors.